

# MIXED METHODS FOR THE VELOCITY-PRESSURE-PSEUDOSTRESS FORMULATION OF THE STOKES EIGENVALUE PROBLEM

FELIPE LEPE, GONZALO RIVERA, AND JESUS VELLOJIN

**ABSTRACT.** In two and three dimensional domains, we analyze mixed finite element methods for a velocity-pressure-pseudostress formulation of the Stokes eigenvalue problem. The methods consist in two schemes: the velocity and pressure are approximated with piecewise polynomial and for the pseudostress we consider two classic families of finite elements for  $H(\text{div})$  spaces: the Raviart-Thomas and the Brezzi-Douglas Marini elements. With the aid of the classic spectral theory for compact operators, we prove that our method does not introduce spurious modes. Also, we obtain convergence and error estimates for the proposed methods. In order to assess the performance of the schemes, we report numerical results to compare the accuracy and robustness between both numerical schemes.

## 1. INTRODUCTION

The Stokes problem is a system of equations that describes the motion of a certain fluid. For a given domain  $\Omega \subset \mathbb{R}^n$ , where  $n \in \{2, 3\}$  with Lipschitz boundary, we are interested in the Stokes eigenvalue problem.

$$(1.1) \quad \begin{cases} -2\mu\Delta \mathbf{u} + \nabla p &= \lambda \mathbf{u} & \text{in } \Omega, \\ \operatorname{div} \mathbf{u} &= 0 & \text{in } \Omega, \\ \mathbf{u} &= \mathbf{0} & \text{on } \partial\Omega, \end{cases}$$

where  $\mu$  is the kinematic viscosity,  $\mathbf{u}$  is the velocity and  $p$  is the pressure.

It is well known that mixed formulations are a suitable alternative to analyze different problems, since the introduction of additional unknowns with physical meaning, allows to obtain more information for certain phenomenons. Hence, the design of finite element approximations has been an important subject of study for mathematicians and engineers, where several families of mixed elements have been developed. For a complete state of art about mixed methods we resort to [5].

In particular, mixed formulations for eigenvalue problems has been well developed in the past years and the theory to study these problems can be found in [4, 22], just for mention the more classic references. On the other hand, concrete

---

2000 *Mathematics Subject Classification.* Primary 35Q35, 65N15, 65N25, 65N30, 65N50, 76D07.

*Key words and phrases.* Stokes equations, eigenvalue problems, error estimates.

The first author was partially supported by ANID-Chile through FONDECYT project 11200529 (Chile).

The second author was supported by ANID-Chile through FONDECYT project 11170534 (Chile).

The third author was partially supported by ANID-Chile through FONDECYT project 1181098 (Chile).

applications for mixed formulations in spectral problems can be found in different contexts as, for instance, [1, 10, 13, 12, 17, 19], where several tools have been implemented as DG methods, VEM methods, FEM, and a posteriori analysis.

In the present work, we consider a tensorial formulation for the Stokes spectral problem. This type of formulation naturally arise when we are interested in the computation of the stress.

More precisely, we will study the Stokes eigenvalue problem with the mixed formulation proposed in [11] for the source problem where, not only the velocity and the pressure are the unknowns as in (1.1), but also the pseudostress tensor (see [9] for further details related to this tensor). With these formulation, clearly the computational costs for the numerical methods increment compared with the classic velocity-pressure formulation, since we need to approximate each component of the pseudostress, each component of the velocity and the scalar associated to the pressure. However, this tensor is an interesting unknown since allows to compute other quantities of interest. For example, in the Stokes flow problems, the pseudostress relates the classic stress and the gradient of the velocity. Hence, with an accurate approximation of the pseudostress we are able to obtain accurate values for these other relevant unknowns.

One of the motivations to analyze the mixed formulation of our work is that allows to deal with eigenfunctions that present a poor regularity compared with those of the classic velocity-pressure formulation, which is a clear advantage when functions of these nature are presented in real applications. Moreover, mixed formulations are flexible in the choice of finite element families to approximate the space  $H(\text{div})$ . In our case, we will consider two families: the Raviart-Thomas elements and the Brezzi-Douglas-Marini elements (see for instance [6, 23]). The aim is to compare the accuracy of these inf-sup stable finite elements to approximate the eigenfunctions and eigenvalues of (1.1). It is well known that BDM schemes are more expensive than RT schemes, which immediately give us the computational costs as first main difference. However, in eigenvalue problems, the orders of convergence and accuracy for the approximation of the spectrum of the solution operators can benefited with more expensive elements. Also, in the present work we perform a theoretical and computational analysis for high order mixed methods for both families of finite elements, which becomes an important feature to compare.

The paper is organized as follows: in Section 2 we introduce the Stokes eigenvalue problem, for two and three dimensions, together with the pseudostress tensor. With suitable Hilbert spaces we derive a variational formulation for (1.1) where the main unknowns are the pseudostress, the velocity and the pressure. We introduce the corresponding solution operators and present an additional regularity result for the eigenfunctions. Finally, a spectral characterization is deduced. Section 3 is the core of our paper, where we introduce the finite element schemes of our analysis. We prove the stability for the discrete eigenvalue problem. Also we introduce the discrete solution operator. In Section 4 we perform the spectral analysis, where convergence and error results for the eigenfunctions and eigenvalues are proved. Finally, in Section 5 we report a series of numerical tests where we confirm our theoretical results, together with a comparison between the mixed schemes of our paper.

We end this section with some of the notations that we will use below. Given any Hilbert space  $X$ , let  $X^2$  and  $\mathbb{X}$  denote, respectively, the space of vectors and tensors

with entries in  $X$ . In particular,  $\mathbb{I}$  is the identity matrix of  $\mathbb{R}^{n \times n}$ , and  $\mathbf{0}$  denotes a generic null vector or tensor. Given  $\boldsymbol{\tau} := (\tau_{ij})$  and  $\boldsymbol{\sigma} := (\sigma_{ij}) \in \mathbb{R}^{n \times n}$ , we define, as usual, the transpose tensor  $\boldsymbol{\tau}^t := (\tau_{ji})$ , the trace  $\text{tr } \boldsymbol{\tau} := \sum_{i=1}^n \tau_{ii}$ , the deviatoric tensor  $\boldsymbol{\tau}^d := \boldsymbol{\tau} - \frac{1}{n}(\text{tr } \boldsymbol{\tau})\mathbb{I}$ , and the tensor inner product  $\boldsymbol{\tau} : \boldsymbol{\sigma} := \sum_{i,j=1}^n \tau_{ij}\sigma_{ij}$ .

Let  $\Omega$  be a polygonal Lipschitz bounded domain of  $\mathbb{R}^n$  with boundary  $\partial\Omega$ . For  $s \geq 0$ ,  $\|\cdot\|_{s,\Omega}$  stands indistinctly for the norm of the Hilbertian Sobolev spaces  $H^s(\Omega)$ ,  $H^s(\Omega)^n$  or  $\mathbb{H}^s(\Omega)$  for scalar, vectorial and tensorial fields, respectively, with the convention  $H^0(\Omega) := L^2(\Omega)$ ,  $[H^0(\Omega)]^n = [L^2(\Omega)]^n$  and  $\mathbb{H}^0(\Omega) := L^2(\Omega)$ . We also define for  $s \geq 0$  the Hilbert space  $\mathbb{H}^s(\text{div}; \Omega) := \{\boldsymbol{\tau} \in \mathbb{H}^s(\Omega) : \text{div } \boldsymbol{\tau} \in [H^s(\Omega)]^n\}$ , whose norm is given by  $\|\boldsymbol{\tau}\|_{\mathbb{H}^s(\text{div}; \Omega)}^2 := \|\boldsymbol{\tau}\|_{s,\Omega}^2 + \|\text{div } \boldsymbol{\tau}\|_{s,\Omega}^2$ .

The relation  $\mathbf{a} \lesssim \mathbf{b}$  indicates that  $\mathbf{a} \leq C\mathbf{b}$ , with a positive constant  $C$  which is independent of  $\mathbf{a}$  and  $\mathbf{b}$ .

## 2. THE MODEL PROBLEM

Let  $\Omega$  be a bounded simply connected polygonal domain with boundary  $\partial\Omega$ . We introduce the pseudostress tensor  $\boldsymbol{\sigma} := 2\mu\nabla\mathbf{u} - p\mathbb{I}$ . Hence, system (1.1) is rewritten as follows:

$$(2.2) \quad \begin{cases} \text{div } \boldsymbol{\sigma} &= -\lambda\mathbf{u} & \text{in } \Omega, \\ \boldsymbol{\sigma} - 2\mu\nabla\mathbf{u} + p\mathbb{I} &= \mathbf{0} & \text{in } \Omega, \\ \text{div } \mathbf{u} &= 0 & \text{in } \Omega, \\ \mathbf{u} &= \mathbf{0} & \text{on } \partial\Omega, \end{cases}$$

where  $\mu$  is the kinematic viscosity,  $\mathbb{I} \in \mathbb{R}^{n \times n}$  is the identity matrix, and  $\text{div}$  must be understood as the divergence of any tensor applied along on each row. As is commented in [11], the pressure and the pseudostress tensor are related through the following identity

$$p = -\frac{1}{n} \text{tr}(\boldsymbol{\sigma}) \quad \text{in } \Omega.$$

This identity holds by the incompressibility condition, together with the identity  $\text{tr}(\nabla\mathbf{u}) = \text{div } \mathbf{u}$ . Hence, problem (2.2) can be rewritten as the following system

$$(2.3) \quad \begin{cases} \text{div } \boldsymbol{\sigma} &= -\lambda\mathbf{u} & \text{in } \Omega, \\ \boldsymbol{\sigma} - 2\mu\nabla\mathbf{u} + p\mathbb{I} &= \mathbf{0} & \text{in } \Omega, \\ p + \frac{1}{n} \text{tr}(\boldsymbol{\sigma}) &= 0 & \text{in } \Omega, \\ \mathbf{u} &= \mathbf{0} & \text{on } \partial\Omega. \end{cases}$$

For the analysis of problem (2.3), we are interested in the following variational formulation: Find  $\lambda \in \mathbb{R}$  and the triplet  $\mathbf{0} \neq (\boldsymbol{\sigma}, p, \mathbf{u}) \in \mathbb{H}(\text{div}, \Omega) \times L^2(\Omega) \times [L^2(\Omega)]^n$  such that

$$(2.4) \quad \frac{1}{2\mu} \int_{\Omega} \boldsymbol{\sigma}^d : \boldsymbol{\tau}^d + \frac{1}{\mu} \int_{\Omega} \left( p + \frac{1}{n} \text{tr}(\boldsymbol{\sigma}) \right) \left( q + \frac{1}{n} \text{tr}(\boldsymbol{\tau}) \right) \\ + \int_{\Omega} \mathbf{u} \cdot \text{div } \boldsymbol{\tau} = 0 \quad \forall (\boldsymbol{\tau}, q) \in \mathbb{H}(\text{div}, \Omega) \times L^2(\Omega),$$

$$(2.5) \quad \int_{\Omega} \mathbf{v} \cdot \text{div } \boldsymbol{\sigma} = -\lambda(\mathbf{u}, \mathbf{v}) \quad \forall \mathbf{v} \in [L^2(\Omega)]^n,$$

It is important to remark that problem (2.4)–(2.5) has a solution, but the uniqueness is not satisfied. To avoid this circumvent, and inspired by [11, Section 2], we consider the following decomposition of  $\mathbb{H}(\text{div}, \Omega) = \mathbb{H}_0 \oplus \mathbb{R}\mathbb{I}$ , where

$$\mathbb{H}_0 := \left\{ \boldsymbol{\tau} \in \mathbb{H}(\mathbf{div}, \Omega) : \int_{\Omega} \text{tr}(\boldsymbol{\tau}) = 0 \right\}.$$

In order to simplify the presentation of the material, we define  $\mathbb{H} := \mathbb{H}_0 \times L^2(\Omega)$  and  $\mathbf{Q}^u := [L^2(\Omega)]^n$ . The bilinear forms  $a : \mathbb{H} \times \mathbb{H} \rightarrow \mathbb{R}$  and  $b : \mathbb{H}(\mathbf{div}, \Omega) \times \mathbf{Q}^u \rightarrow \mathbb{R}$  are defined as follows:

$$a((\boldsymbol{\xi}, r), (\boldsymbol{\tau}, q)) := \frac{1}{2\mu} \int_{\Omega} \boldsymbol{\xi}^d : \boldsymbol{\tau}^d + \frac{\gamma}{\mu} \left( p + \frac{1}{n} \text{tr}(\boldsymbol{\xi}) \right) \left( q + \frac{1}{n} \text{tr}(\boldsymbol{\tau}) \right),$$

and

$$b(\boldsymbol{\xi}, \mathbf{v}) := \int_{\Omega} \mathbf{v} \cdot \mathbf{div} \boldsymbol{\xi}.$$

According to [11, Lemma 2.2], we have that any solution of problem (2.4)–(2.5) with  $\boldsymbol{\sigma} \in \mathbb{H}_0$  is also solution of:

$$(2.6) \quad a((\boldsymbol{\sigma}, p), (\boldsymbol{\tau}, q)) + b(\boldsymbol{\tau}, \mathbf{u}) = 0 \quad \forall (\boldsymbol{\tau}, q) \in \mathbb{H},$$

$$(2.7) \quad b(\boldsymbol{\sigma}, \mathbf{v}) = -\lambda(\mathbf{u}, \mathbf{v}) \quad \forall \mathbf{v} \in \mathbf{Q}^u,$$

with  $\gamma = 1$ , and also, any solution of (2.6)–(2.7) is also solution of problem (2.4)–(2.5).

It is possible to consider an alternative reduced formulation for our problem (2.6)–(2.7), which only depends on the stress tensor and the velocity.

With the space  $\mathbb{H}_0$  at hand, we consider the following problem: find  $\lambda \in \mathbb{R}$  and  $\mathbf{0} \neq (\boldsymbol{\sigma}, \mathbf{u}) \in \mathbb{H}_0 \times \mathbf{Q}^u$  such that

$$(2.8) \quad a_0(\boldsymbol{\sigma}, \boldsymbol{\tau}) + b(\boldsymbol{\tau}, \mathbf{u}) = 0 \quad \forall \boldsymbol{\tau} \in \mathbb{H}_0,$$

$$(2.9) \quad b(\boldsymbol{\sigma}, \mathbf{v}) = -\lambda(\mathbf{u}, \mathbf{v}) \quad \forall \mathbf{v} \in \mathbf{Q}^u,$$

where  $a_0 : \mathbb{H}_0 \times \mathbb{H}_0 \rightarrow \mathbb{R}$  is a bounded bilinear form defined by

$$a_0(\boldsymbol{\xi}, \boldsymbol{\tau}) := \frac{1}{2\mu} \int_{\Omega} \boldsymbol{\xi}^d : \boldsymbol{\tau}^d \quad \forall (\boldsymbol{\xi}, \boldsymbol{\tau}) \in \mathbb{H}_0 \times \mathbb{H}_0.$$

We remark that the pressure can be recovered with the third equation of system (2.3).

**Remark 2.1.** *It is easy to check that if  $(\lambda, \boldsymbol{\sigma}, p, \mathbf{u}) \in \mathbb{R} \times \mathbb{H} \times \mathbf{Q}$  is a solution of problem (2.6)–(2.7) if and only if  $(\lambda, \boldsymbol{\sigma}, \mathbf{u}) \in \mathbb{R} \times \mathbb{H}_0 \times \mathbf{Q}$  is a solution of problem (2.8)–(2.9) and  $p = -\frac{1}{n} \text{tr}(\boldsymbol{\sigma})$  (see [11, Lemma 2.3]).*

For the analysis of the mixed problem (2.8)–(2.9) we invoke the following result (see [5, Ch. 4, Proposition 3.1])

$$(2.10) \quad \|\boldsymbol{\tau}\|_{0,\Omega}^2 \lesssim \|\boldsymbol{\tau}^d\|_{0,\Omega}^2 + \|\mathbf{div} \boldsymbol{\tau}\|_{0,\Omega}^2.$$

Let us introduce the kernel of the operator induced by  $b(\cdot, \cdot)$

$$\mathcal{V} := \{ \boldsymbol{\tau} \in \mathbb{H}_0 : b(\boldsymbol{\tau}, \mathbf{v}) = 0 \quad \forall \mathbf{v} \in \mathbf{Q} \} = \{ \boldsymbol{\tau} \in \mathbb{H}_0 : \mathbf{div} \boldsymbol{\tau} = \mathbf{0} \}.$$

With the aid of (2.10) it is easy to check that  $a_0(\cdot, \cdot)$  is coercive in  $\mathcal{V}$  (see [11, Subsection 2.3])

$$a_0(\boldsymbol{\tau}, \boldsymbol{\tau}) \geq \alpha \|\boldsymbol{\tau}\|_{\text{div}}^2 \quad \forall \boldsymbol{\tau} \in \mathcal{V},$$

where it can be proved that  $\alpha = C/2\mu$ , with  $C$  being the positive constant provided by (2.10).



On the other hand, there exists a positive constant  $\beta$  such that the following inf-sup condition for  $b(\cdot, \cdot)$  holds (see [11, Theorem 2.1])

$$\sup_{\mathbf{0} \neq \boldsymbol{\tau} \in \mathbb{H}_0} \frac{b(\boldsymbol{\tau}, \mathbf{v})}{\|\boldsymbol{\tau}\|_{\text{div}, \Omega}} \geq \beta \|\mathbf{v}\|_{0, \Omega} \quad \forall \mathbf{v} \in \mathbf{Q}^u.$$

With this results at hand, we are in position to introduce the solution operator

$$\begin{aligned} \mathbf{T} : \mathbf{Q}^u &\rightarrow \mathbf{Q}^u, \\ \mathbf{f} &\mapsto \mathbf{T}\mathbf{f} := \widehat{\mathbf{u}}, \end{aligned}$$

where the pair  $(\widehat{\boldsymbol{\sigma}}, \widehat{\mathbf{u}})$  is the solution of the following source problem

$$(2.11) \quad a_0(\widehat{\boldsymbol{\sigma}}, \boldsymbol{\tau}) + b(\boldsymbol{\tau}, \widehat{\mathbf{u}}) = 0 \quad \forall \boldsymbol{\tau} \in \mathbb{H}_0,$$

$$(2.12) \quad b(\widehat{\boldsymbol{\sigma}}, \mathbf{v}) = -(\mathbf{f}, \mathbf{v}) \quad \forall \mathbf{v} \in \mathbf{Q}^u,$$

Notice that  $\mathbf{T}$  is well defined due the Babuška-Brezzi theory and we have the follows estimate

$$\|\widehat{\boldsymbol{\sigma}}\|_{\text{div}, \Omega} + \|\widehat{\mathbf{u}}\|_{0, \Omega} \lesssim \|\mathbf{f}\|_{0, \Omega}.$$

Moreover, it is easy to check that  $\mathbf{T}$  is self-adjoint respect the  $[\mathbf{L}^2]^n$ - inner product. Indeed, given  $\mathbf{f}, \widehat{\mathbf{f}} \in \mathbf{Q}^u$ , let  $(\widehat{\boldsymbol{\sigma}}, \widehat{\mathbf{u}}) \in \mathbb{H}_0 \times \mathbf{Q}^u$  and  $(\widetilde{\boldsymbol{\sigma}}, \widetilde{\mathbf{u}}) \in \mathbb{H}_0 \times \mathbf{Q}^u$  be the solutions to problem (2.11)–(2.12) with right hand sides  $\mathbf{f}$  and  $\widehat{\mathbf{f}}$ , respectively. Assume that that  $\mathbf{T}\mathbf{f} = \widehat{\mathbf{u}}$  and  $\mathbf{T}\widehat{\mathbf{f}} = \widetilde{\mathbf{u}}$ . The symmetry of  $a(\cdot, \cdot)$  and  $(\cdot, \cdot)_{0, \Omega}$  implies that

$$(\mathbf{f}, \mathbf{T}\widehat{\mathbf{f}})_{0, \Omega} = (\mathbf{f}, \widetilde{\mathbf{u}})_{0, \Omega} = -(a(\widehat{\boldsymbol{\sigma}}, \widetilde{\mathbf{u}}) + b(\widetilde{\mathbf{u}}, \widehat{\boldsymbol{\sigma}}) + b(\widehat{\boldsymbol{\sigma}}, \widetilde{\mathbf{u}})) = (\widetilde{\mathbf{f}}, \widehat{\mathbf{u}})_{0, \Omega} = (\mathbf{T}\widehat{\mathbf{f}}, \mathbf{f})_{0, \Omega}.$$

We observe that  $(\lambda, (\boldsymbol{\sigma}, \mathbf{u})) \in \mathbb{R} \times \mathbb{H}_0 \times \mathbf{Q}^u$  solves (2.8)–(2.9) if and only if  $(\kappa, \mathbf{u})$  is an eigenpair of  $\mathbf{T}$ , i.e.

$$\mathbf{T}\mathbf{u} = \kappa \mathbf{u} \quad \text{with } \kappa := \frac{1}{\lambda}.$$

The next step in our analysis is to obtain an additional regularity result for our eigenfunctions. To do this task, we consider the following problem: given  $\mathbf{f} \in \mathbf{L}^2(\Omega)^n$ , let  $(\widetilde{\mathbf{u}}, \widetilde{\boldsymbol{\sigma}}) \in [\mathbf{H}^1(\Omega)]^n \times \mathbb{H}(\text{div}; \Omega)$  be the solution of the following problem

$$\begin{cases} -\text{div } \widetilde{\boldsymbol{\sigma}} &= \mathbf{f} & \text{in } \Omega, \\ \frac{1}{2\mu} \widetilde{\boldsymbol{\sigma}}^d &= \nabla \widetilde{\mathbf{u}} & \text{in } \Omega, \\ \widetilde{\boldsymbol{\sigma}} &= \mathbf{0} & \text{on } \partial\Omega, \\ \widetilde{\mathbf{u}} &= \mathbf{0} & \text{on } \partial\Omega. \end{cases}$$

Now, using the relation between incompressible elasticity and the Stokes problem and according to [14] we conclude that: there exists  $s \in (0, 1)$  such that  $\widehat{\mathbf{u}} \in [\mathbf{H}^{1+s}(\Omega)]^n$  and

$$(2.13) \quad \|\widehat{\boldsymbol{\sigma}}\|_{s, \Omega} + \|\widehat{\mathbf{u}}\|_{1+s, \Omega} \lesssim \|\mathbf{f}\|_{0, \Omega}.$$

Hence, the compactness of  $\mathbf{T}$  is a direct consequence of the previous regularity result. Finally, we have the following spectral characterization.

**Theorem 2.1.** *The spectrum of  $\mathbf{T}$  satisfies  $\text{sp}(\mathbf{T}) = \{0\} \cup \{\mu_k\}_{k \in \mathbb{N}}$ , where  $\{\mu_k\}_{k \in \mathbb{N}} \in (0, 1)$  is a sequence of real positive eigenvalues which converges to zero, repeated according their respective multiplicities. In addition, the following additional regularity result holds true for eigenfunctions*

$$\|\boldsymbol{\sigma}\|_{s, \Omega} + \|\mathbf{u}\|_{1+s, \Omega} \lesssim \|\mathbf{u}\|_{0, \Omega}.$$

We have from Remark 2.1 that problems (2.6)–(2.7) and (2.8)–(2.9) are equivalent. However, the finite element discretizations for these problems are not equivalent (cf. Section 3). Hence, to obtain error estimates for our methods, we need to consider an additional solution operator associated with the problem (2.6)–(2.7).

Now, let  $\tilde{\mathbf{T}}$  be the solution operator defined by

$$\begin{aligned}\tilde{\mathbf{T}} : \mathbf{Q}^u &\rightarrow \mathbf{Q}^u, \\ \mathbf{f} &\mapsto \tilde{\mathbf{T}}\mathbf{f} := \tilde{\mathbf{u}},\end{aligned}$$

where  $(\tilde{\boldsymbol{\sigma}}, \tilde{p}, \tilde{\mathbf{u}})$  is the solution of the following source problem

$$\begin{aligned}a((\tilde{\boldsymbol{\sigma}}, \tilde{p}), (\boldsymbol{\tau}, q)) + b(\boldsymbol{\tau}, \tilde{\mathbf{u}}) &= 0 \quad \forall (\boldsymbol{\tau}, q) \in \mathbb{H}, \\ b(\tilde{\boldsymbol{\sigma}}, \mathbf{v}) &= -(\tilde{\mathbf{f}}, \mathbf{v}) \quad \forall \mathbf{v} \in \mathbf{Q}^u.\end{aligned}$$

Thanks to the Remark 2.1 and the fact that the operator  $\mathbf{T}$  is well-defined, we have that also  $\tilde{\mathbf{T}}$  is well defined (see [11, Theorem 2.2]) and there holds

$$\|\tilde{\boldsymbol{\sigma}}\|_{\mathbf{div}, \Omega} + \|\tilde{p}\|_{0, \Omega} + \|\tilde{\mathbf{u}}\|_{0, \Omega} \lesssim \|\tilde{\mathbf{f}}\|_{0, \Omega}.$$

Moreover, it is easy to check that  $\tilde{\mathbf{T}}$  is self-adjoint respect the  $[\mathbf{L}^2(\Omega)]^n$ - inner product and we observe that  $(\lambda, (\boldsymbol{\sigma}, p, \mathbf{u})) \in \mathbb{R} \times \mathbb{H} \times \mathbf{Q}^u$  solves (2.6)–(2.7) if and only if  $(\kappa, \mathbf{u})$  is an eigenpair of  $\tilde{\mathbf{T}}$ . Hence,  $\tilde{\mathbf{T}}$  is compact and  $\text{sp}(\tilde{\mathbf{T}}) = \text{sp}(\mathbf{T}) = \{0\} \cup \{\mu_k\}_{k \in \mathbb{N}}$

### 3. THE MIXED FINITE ELEMENT METHOD

The present section deals with the finite element approximation for the eigenvalue problem. To do this task, we begin by introducing a regular family of triangulations of  $\Omega$  denoted by  $\{\mathcal{T}_h\}_{h>0}$ . Let  $h_T$  the diameter of a triangle  $T$  of the triangulation and let us define  $h := \max\{h_T : T \in \mathcal{T}_h\}$ .

Given an integer  $\ell \geq 0$  and a subset  $D$  of  $\mathbb{R}^n$ , we denote by  $\mathbb{P}_\ell(S)$  the space of polynomials of degree at most  $\ell$  defined in  $D$ .

**3.1. The finite element spaces.** In our study, we consider two numerical schemes that only differ in the space that approximates the pseudostress. Hence, we only refer to  $\mathbb{H}_h^\sigma$  to the finite element space related to the approximation of  $\boldsymbol{\sigma}$ . For the velocity field we consider the space  $\mathbf{Q}_h^u$  and for the pressure  $Q_h^p$ . In what follows we specify each of these finite dimensional spaces.

For  $k \geq 0$  we define the local Raviart-Thomas space of order  $k$  as follows (see [5])

$$\mathbb{RT}_k(T) = [\mathbb{P}_k(T)]^n \oplus \mathbb{P}_k(T)\mathbf{x},$$

where if  $\mathbf{t}$  denotes the transpose operator,  $\mathbf{x}^{\mathbf{t}}$  represents a generic vector of  $\mathbb{R}^n$ . Hence, the global Raviart-Thomas is defined by

$$\mathbb{RT}_k(\mathcal{T}_h) := \{\boldsymbol{\tau} \in \mathbb{H}(\mathbf{div}, \Omega) : \boldsymbol{\tau}|_T^{\mathbf{t}} \in \mathbb{RT}_k(T), \forall T \in \mathcal{T}_h\}.$$

More precisely, in the definition above  $\boldsymbol{\tau}|_T^{\mathbf{t}}$  must be understood as  $(\tau_{i1}, \tau_{i2})^{\mathbf{t}} \in \mathbb{RT}_k(T)$  for all  $i \in \{1, 2\}$  when  $n = 2$ , and  $(\tau_{j1}, \tau_{j2}, \tau_{j3})^{\mathbf{t}} \in \mathbb{RT}_k(T)$  for all  $j \in \{1, 2, 3\}$  when  $n = 3$ .

On the other hand, we define the space of piecewise polynomials of degree at most  $k$

$$\mathbb{P}_k(\mathcal{T}_h) := \{v \in \mathbf{L}^2(\Omega) : v|_T \in \mathbb{P}_k(T) \forall T \in \mathcal{T}_h\}.$$

In addition, we introduce the Brezzi-Douglas-Marini finite element space [6],

$$\mathbb{BDM}_k := [\mathbb{P}_k(\mathcal{T}_h)]^n \cap \mathbb{H} \text{ with } k \geq 1.$$

It is well known from the literature that  $\mathbb{RT}_{k-1} \subset \mathbb{BDM}_k \subset \mathbb{RT}_k$  for all  $k \geq 1$  (see [5, Section 2]). Moreover, the number of degrees of freedom per edge is the same for both finite elements, however, the number of internal degrees of freedom of Brezzi-Douglas-Marini ( $\mathbb{BDM}_k$ ) elements is less than that of standard finite elements of the same order such as Raviart-Thomas ( $\mathbb{RT}_k$ ). A count of the internal degrees of freedom for  $n = 2$  gives

$$\mathbb{BDM}_k : 2(k-1)(k+1). \quad \mathbb{RT}_k : 2k(k+1),$$

and for  $n = 3$

$$\mathbb{BDM}_k : \frac{3}{2}(k-1)(k+1)(k+2). \quad \mathbb{RT}_k : \frac{3}{2}k(k+1)(k+2),$$

**3.2. Approximation errors.** In the following, some approximation results for discrete spaces are presented. To make matters precise, since we consider two spaces to approximate the pseudostress tensor, we need to introduce suitable interpolators for each finite element space, namely, Raviart-Thomas and BDM spaces. We begin with the classical approximation property for piecewise polynomials (see [3]). Let  $\mathcal{R}_h : [\mathbb{L}^2(\Omega)]^n \rightarrow [\mathbb{P}_k(\mathcal{T}_h)]^n$ . The following estimate is true.

$$(3.14) \quad \|\mathbf{v} - \mathcal{R}_h \mathbf{v}\|_{0,\Omega} \lesssim h^{\min\{t,k+1\}} \|\mathbf{v}\|_{t,\Omega} \quad \forall t \in [\mathbb{H}^t(\Omega)]^n \cap [\mathbb{L}^2(\Omega)]^n.$$

For the Raviart-Thomas spaces, we have the following approximation results: let  $\Pi_h^{\mathbb{RT}} : [\mathbb{H}^t(\Omega)]^{n \times n} \rightarrow \mathbb{RT}_k$  be the tensorial version of the Raviart-Thomas interpolation operator, which satisfies the following classical error estimate, see [7, 24],

$$(3.15) \quad \|\boldsymbol{\tau} - \Pi_h^{\mathbb{RT}} \boldsymbol{\tau}\|_{0,\Omega} \lesssim h^{\min\{t,k+1\}} \|\boldsymbol{\tau}\|_{t,\Omega} \quad \forall \boldsymbol{\tau} \in [\mathbb{H}^t(\Omega)]^{n \times n}, \quad t \geq 1.$$

Also, thanks to the commutative diagram, if  $\text{div } \boldsymbol{\tau} \in [\mathbb{H}^r(\Omega)]^n$  with  $r \geq 0$  we have the following result

$$(3.16) \quad \|\text{div}(\boldsymbol{\tau} - \Pi_h^{\mathbb{RT}} \boldsymbol{\tau})\|_{0,\Omega} \lesssim h^{\min\{r,k+1\}} \|\text{div } \boldsymbol{\tau}\|_{r,\Omega}.$$

Moreover,  $\Pi_h^{\mathbb{RT}}$  can also be defined as  $\Pi_h^{\mathbb{RT}} : [\mathbb{H}^t(\Omega)]^{n \times n} \cap \mathbb{H}(\text{div}, \Omega) \rightarrow \mathbb{RT}_k$  for all  $t \in (0, 1]$ , and we have the following estimate

$$(3.17) \quad \|\boldsymbol{\tau} - \Pi_h^{\mathbb{RT}} \boldsymbol{\tau}\|_{0,\Omega} \lesssim h^t (\|\boldsymbol{\tau}\|_{t,\Omega} + \|\text{div } \boldsymbol{\tau}\|_{0,\Omega}) \quad \forall \boldsymbol{\tau} \in [\mathbb{H}^t(\Omega)]^{n \times n} \cap \mathbb{H}(\text{div}, \Omega) \quad t \in (0, 1].$$

For the BDM spaces, we have the following properties: let  $\ell \geq 1$  and let  $\Pi_h^{\mathbb{BDM}} : [\mathbb{H}^t(\Omega)]^{n \times n} \rightarrow \mathbb{BDM}_\ell$  be the tensorial version of the BDM-interpolation operator, which satisfies the following classical error estimate, see [15, Theorem 3.16],

$$(3.18) \quad \|\boldsymbol{\tau} - \Pi_h^{\mathbb{BDM}} \boldsymbol{\tau}\|_{0,\Omega} \lesssim h^{\min\{t,\ell+1\}} \|\boldsymbol{\tau}\|_{t,\Omega} \quad \forall \boldsymbol{\tau} \in [\mathbb{H}^t(\Omega)]^{n \times n}, \quad t > 1/2.$$

Also, for less regular tensorial fields we have the following estimate

$$(3.19) \quad \|\boldsymbol{\tau} - \Pi_h^{\mathbb{BDM}} \boldsymbol{\tau}\|_{0,\Omega} \lesssim h^t (\|\boldsymbol{\tau}\|_{t,\Omega} + \|\text{div } \boldsymbol{\tau}\|_{0,\Omega}) \quad \forall \boldsymbol{\tau} \in [\mathbb{H}^t(\Omega)]^{n \times n} \cap \mathbb{H}(\text{div}, \Omega), \quad t \in (0, 1/2].$$

Moreover, the following commuting diagram property holds true:

$$(3.20) \quad \|\text{div}(\boldsymbol{\tau} - \Pi_h^{\mathbb{BDM}} \boldsymbol{\tau})\|_{0,\Omega} = \|\text{div } \boldsymbol{\tau} - \mathcal{R}_h \text{div } \boldsymbol{\tau}\|_{0,\Omega} \lesssim h^{\min\{t,\ell\}} \|\text{div } \boldsymbol{\tau}\|_{t,\Omega},$$

for  $\text{div } \boldsymbol{\tau} \in [\mathbb{H}^t(\Omega)]^n$  and  $\mathcal{R}_h$  being the  $[\mathbb{L}^2(\Omega)]^n$ -orthogonal projection onto  $[\mathbb{P}_{\ell-1}(\mathcal{T}_h)]^n$ .

We conclude this section by introducing the following notations

$$\mathbb{H}_{0,h}^\sigma := \left\{ \boldsymbol{\tau} \in \bar{\mathbb{H}}_h : \int_{\Omega} \text{tr}(\boldsymbol{\tau}) = 0 \right\},$$

where  $\bar{\mathbb{H}}_h \in \{\text{RT}_k, \text{BDM}_{k+1}\}$ . Also, we define  $Q_h^p := \mathbb{P}_k(\mathcal{T}_h)$ ,  $\mathbf{Q}_h^u := [\mathbb{P}_k(\mathcal{T}_h)]^n$ . and  $\mathbb{H}_h := \mathbb{H}_{0,h}^\sigma \times Q_h^p$ .

Therefore, as a consequence of (3.14)–(3.20), we have the following approximation properties for  $k \geq 0$ : For each  $t > 0$  and for each  $\boldsymbol{\tau} \in \mathbb{H}^t(\Omega) \cap \mathbb{H}_0$  with  $\text{div } \boldsymbol{\tau} \in [\text{H}^t(\Omega)]^n$  there exists  $\boldsymbol{\tau}_h \in \mathbb{H}_0^\sigma$  such that

$$(3.21) \quad \|\boldsymbol{\tau} - \boldsymbol{\tau}_h\|_{\text{div}, \Omega} \lesssim h^{\min\{t, k+1\}} (\|\boldsymbol{\tau}\|_{t, \Omega} + \|\text{div } \boldsymbol{\tau}\|_{t, \Omega}).$$

For  $q \in Q^p$  there exists  $q_h \in Q_h^p$  such that

$$(3.22) \quad \|q - q_h\|_{0, \Omega} \lesssim h^{\min\{t, k+1\}} \|q\|_{t, \Omega}.$$

For  $\mathbf{v} \in [\text{H}^t(\Omega)]^n$  there exists  $\mathbf{v}_h \in \mathbf{Q}_h^u$  such that

$$(3.23) \quad \|\mathbf{v} - \mathbf{v}_h\|_{0, \Omega} \lesssim h^{\min\{t, k+1\}} \|\mathbf{v}\|_{t, \Omega}.$$

**3.3. The discrete eigenvalue problems.** As we claim in Section 2, discrete counterparts of problems (2.6)–(2.7) and (2.8)–(2.9) are not equivalent (see [11, Lemma 3.1] for further details). Hence, we need to analyze each discrete eigenvalue problem by separated.

With the discrete spaces defined above, we are in position to introduce the discretization of problem (2.6)–(2.7): Find  $\lambda_h \in \mathbb{R}$  and  $\mathbf{0} \neq (\boldsymbol{\sigma}_h, p_h, \mathbf{u}_h) \in \mathbb{H}_h \times \mathbf{Q}_h^u$  such that

$$(3.24) \quad a((\boldsymbol{\sigma}_h, p_h), (\boldsymbol{\tau}_h, q_h)) + b(\boldsymbol{\tau}_h, \mathbf{u}_h) = 0 \quad \forall (\boldsymbol{\tau}_h, q_h) \in \mathbb{H}_h,$$

$$(3.25) \quad b(\boldsymbol{\sigma}_h, \mathbf{v}_h) = -\lambda_h(\mathbf{u}_h, \mathbf{v}_h) \quad \forall \mathbf{v}_h \in \mathbf{Q}_h^u.$$

Similarly as in the continuous case, it is possible to consider a reduced formulation for the discrete eigenvalue problem. These reduced discrete problem reads as follows: find  $\lambda_h \in \mathbb{R}$  and  $\mathbf{0} \neq (\boldsymbol{\sigma}_h, \mathbf{u}_h) \in \mathbb{H}_{0,h}^\sigma \times \mathbf{Q}_h^u$  such that

$$(3.26) \quad a_0(\boldsymbol{\sigma}_h, \boldsymbol{\tau}_h) + b(\boldsymbol{\tau}_h, \mathbf{u}_h) = 0 \quad \forall \boldsymbol{\tau}_h \in \mathbb{H}_{0,h}^\sigma,$$

$$(3.27) \quad b(\boldsymbol{\sigma}_h, \mathbf{v}_h) = -\lambda(\mathbf{u}_h, \mathbf{v}_h) \quad \forall \mathbf{v}_h \in \mathbf{Q}_h^u.$$

It has been proved in [11, Lemma 3.2] that there exists a positive constant  $\beta$ , independent of  $h$ , such that the following inf-sup condition holds

$$\sup_{\mathbf{0} \neq \boldsymbol{\tau}_h \in \mathbb{H}_{0,h}^\sigma} \frac{b(\boldsymbol{\tau}_h, \mathbf{v}_h)}{\|\boldsymbol{\tau}_h\|_{\text{div}, \Omega}} \geq \beta \|\mathbf{v}_h\|_{0, \Omega} \quad \forall \mathbf{v}_h \in \mathbf{Q}_h^u.$$

On the other hand, the discrete kernel of  $b(\cdot, \cdot)$  (namely, the kernel of the operator induced by  $b(\cdot, \cdot)$ ) is defined by

$$\mathcal{V}_h := \{\boldsymbol{\tau} \in \mathbb{H}_{0,h}^\sigma : b(\boldsymbol{\tau}, \mathbf{v}) = \mathbf{0} \ \forall \mathbf{v} \in \mathbf{Q}_h^u\} = \{\boldsymbol{\tau} \in \mathbb{H}_{0,h}^\sigma : \text{div } \boldsymbol{\tau} = \mathbf{0} \text{ in } \Omega\}.$$

In [11, Theorem 3.1] the authors have stated that  $a_0(\cdot, \cdot)$  is coercive in  $\mathcal{V}_h$  and that  $b(\cdot, \cdot)$  satisfies the corresponding discrete inf-sup condition.

With these ingredients at hand, we are in position to introduce the discrete solution operator associated to (3.26)–(3.27)

$$\begin{aligned} T_h : \mathbf{Q}^u &\rightarrow \mathbf{Q}_h^u, \\ f &\mapsto T_h f := \hat{\mathbf{u}}_h, \end{aligned}$$

where  $(\widehat{\boldsymbol{\sigma}}_h, \widehat{\mathbf{u}}_h)$  is the solution of the following source problem

$$\begin{aligned} a_0(\widehat{\boldsymbol{\sigma}}_h, \boldsymbol{\tau}_h) + b(\boldsymbol{\tau}_h, \widehat{\mathbf{u}}_h) &= 0 & \forall \boldsymbol{\tau}_h \in \mathbb{H}_{0,h}^\sigma \\ b(\widehat{\boldsymbol{\sigma}}_h, \mathbf{v}_h) &= -(\mathbf{f}, \mathbf{v}_h) & \forall \mathbf{v}_h \in \mathbf{Q}_h^u, \end{aligned}$$

which according to the Babuška-Brezzi theory, is well posed (see [5]) and the following estimate holds.

$$\|\widehat{\boldsymbol{\sigma}}_h\|_{\text{div},\Omega} + \|\widehat{\mathbf{u}}_h\|_{0,\Omega} \lesssim \|\mathbf{f}\|_{0,\Omega},$$

where the hidden constant is independent of  $h$ .

As presented in [11, Lemma 3.1], a necessary condition for discrete problem (3.24)–(3.25) and problem (3.26)–(3.27) to be equivalent, is that  $\text{tr}(\mathbb{H}_{0,h}^\sigma) \subset Q_h^p$  and since in this case, this condition does not hold, we need to define the following discrete solution operator  $\widetilde{\mathbf{T}}_h$  associated with the problem (3.24)–(3.25).

$$\begin{aligned} \widetilde{\mathbf{T}}_h : \mathbf{Q}^u &\rightarrow \mathbf{Q}_h^u \\ \widetilde{\mathbf{f}} &\mapsto \widetilde{\mathbf{T}}_h \widetilde{\mathbf{f}} := \widetilde{\mathbf{u}}_h, \end{aligned}$$

where the triplet  $(\widetilde{\boldsymbol{\sigma}}_h, \widetilde{p}_h, \widetilde{\mathbf{u}}_h)$  is the solution of the following source problem

$$\begin{aligned} a((\widetilde{\boldsymbol{\sigma}}_h, \widetilde{p}_h), (\boldsymbol{\tau}_h, q_h)) + b(\boldsymbol{\tau}_h, \widetilde{\mathbf{u}}_h) &= 0 & \forall (\boldsymbol{\tau}_h, q_h) \in \mathbb{H}_h \\ b(\widetilde{\boldsymbol{\sigma}}_h, \mathbf{v}_h) &= -(\widetilde{\mathbf{f}}, \mathbf{v}_h) & \forall \mathbf{v}_h \in \mathbf{Q}_h^u. \end{aligned}$$

Observe that [11, Theorem 3.3] guarantees that  $\widetilde{\mathbf{T}}_h$  is well-defined and

$$\|\widetilde{\boldsymbol{\sigma}}_h\|_{\text{div},\Omega} + \|\widetilde{p}_h\|_{0,\Omega} + \|\widetilde{\mathbf{u}}_h\|_{0,\Omega} \lesssim \|\widetilde{\mathbf{f}}\|_{0,\Omega},$$

where the hidden constant is independent of  $h$ .

We are in position to establish the following approximation result

**Lemma 3.1.** *Let  $\mathbf{f} \in \mathbf{Q}^u$ . The following best approximation estimates hold*

$$\|(\mathbf{T} - \mathbf{T}_h)\mathbf{f}\|_{0,\Omega} \lesssim \inf_{\boldsymbol{\tau}_h \in \mathbb{H}_{0,h}^\sigma} \|\widehat{\boldsymbol{\sigma}} - \boldsymbol{\tau}_h\|_{\text{div},\Omega} + \inf_{\mathbf{v}_h \in \mathbf{Q}_h^u} \|\widehat{\mathbf{u}} - \mathbf{v}_h\|_{0,\Omega},$$

and

$$\|(\widetilde{\mathbf{T}} - \widetilde{\mathbf{T}}_h)\mathbf{f}\|_{0,\Omega} \lesssim \inf_{\boldsymbol{\tau}_h \in \mathbb{H}_{0,h}^\sigma} \|\widetilde{\boldsymbol{\sigma}} - \boldsymbol{\tau}_h\|_{\text{div},\Omega} + \inf_{q_h \in Q_h^p} \|\widetilde{p} - q_h\|_{0,\Omega} + \inf_{\mathbf{v}_h \in \mathbf{Q}_h^u} \|\widetilde{\mathbf{u}} - \mathbf{v}_h\|_{0,\Omega},$$

where the hidden constant is independent of  $h$ .

*Proof.* Let  $\mathbf{f} \in \mathbf{Q}^u$  be such that  $\mathbf{T}\mathbf{f} = \widehat{\mathbf{u}}$  and  $\mathbf{T}_h\mathbf{f} = \widehat{\mathbf{u}}_h$  where  $\widehat{\mathbf{u}}$  is the solution of (2.11)–(2.12) and  $\widehat{\mathbf{u}}_h$  is the solution of (3.26)–(3.27). We remark that  $\widehat{\mathbf{u}}_h$  is the finite element approximation of  $\widehat{\mathbf{u}}$  through the scheme  $\mathbb{H}_{0,h}^\sigma \times \mathbf{Q}_h^u$ .

Hence, applying [11, Theorem 3.1] we have immediately that

$$\|(\mathbf{T} - \mathbf{T}_h)\mathbf{f}\|_{0,\Omega} = \|\widehat{\mathbf{u}} - \widehat{\mathbf{u}}_h\|_{0,\Omega} \lesssim \inf_{\boldsymbol{\tau}_h \in \mathbb{H}_{0,h}^\sigma} \|\widehat{\boldsymbol{\sigma}} - \boldsymbol{\tau}_h\|_{\text{div},\Omega} + \inf_{\mathbf{v}_h \in \mathbf{Q}_h^u} \|\widehat{\mathbf{u}} - \mathbf{v}_h\|_{0,\Omega},$$

where the hidden constant is independent of  $h$ .

For the approximation error  $\|(\widetilde{\mathbf{T}} - \widetilde{\mathbf{T}}_h)\mathbf{f}\|_{0,\Omega}$  the derivation is similar as the previous estimate. This concludes the proof.  $\square$

We remark that Lemma 3.1 is a general result where the choice of the finite element scheme has not influence. If we are more specific in the numerical scheme, the lemma above becomes into an error estimate for each scheme.

Since we are dealing with two numerical schemes and two discrete eigenvalue problems, as corollaries, we derived the following results. The first corresponds to the approximation error between  $\mathbf{T}$  and  $\mathbf{T}_h$ .

**Corollary 3.1** (Approximation between  $\mathbf{T}$  and  $\mathbf{T}_h$ ). *Let  $\mathbf{f} \in \mathbf{Q}^u$ . If the approximation scheme  $[\mathbb{P}_k]^n\text{-RT}_k$  is considered, then there holds*

$$\|(\mathbf{T} - \mathbf{T}_h)\mathbf{f}\|_{0,\Omega} \lesssim h^s \|\mathbf{f}\|_{0,\Omega}.$$

*Otherwise, if the scheme is  $[\mathbb{P}]_k^n\text{-BDM}_{k+1}$ , there holds*

$$\|(\mathbf{T} - \mathbf{T}_h)\mathbf{f}\|_{0,\Omega} \lesssim h^s \|\mathbf{f}\|_{0,\Omega}.$$

*where, in each estimate, the hidden constant is independent of  $h$ .*

*Proof.* The proof follows from (2.13), the first estimate of Lemma 3.1, the approximation properties (3.21) and (3.23)  $\square$

Now we present the analogous of Corollary 3.1, but for the error between  $\tilde{\mathbf{T}}$  and  $\tilde{\mathbf{T}}_h$ . The proof follows the same arguments of corollary above, so we skip the details.

**Corollary 3.2** (Approximation between  $\tilde{\mathbf{T}}$  and  $\tilde{\mathbf{T}}_h$ ). *Let  $\mathbf{f} \in \mathbf{Q}^u$ . If the approximation scheme  $[\mathbb{P}_k]^n\text{-P}_k\text{-RT}_k$  is considered, then there holds*

$$\|(\tilde{\mathbf{T}} - \tilde{\mathbf{T}}_h)\mathbf{f}\|_{0,\Omega} \lesssim h^s \|\mathbf{f}\|_{0,\Omega}.$$

*Otherwise, if the scheme is  $[\mathbb{P}]_k^n\text{-P}_k\text{-BDM}_{k+1}$ , there holds*

$$\|(\tilde{\mathbf{T}} - \tilde{\mathbf{T}}_h)\mathbf{f}\|_{0,\Omega} \lesssim h^s \|\mathbf{f}\|_{0,\Omega}.$$

*where, in each estimate, the hidden constant is independent of  $h$ .*

#### 4. CONVERGENCE AND ERROR ESTIMATES

In this section we will analyze the convergence of the mixed method and derive error estimates for the eigenvalues and eigenfunctions. We remark that, for both of the numerical schemes considered in our paper, these results are valid. Hence, to simplify the presentation of our results, we will prove our results in a reduced formulation. Due the compactness of  $\mathbf{T}$  and  $\tilde{\mathbf{T}}$ , the convergence of the eigenvalues is obtained by means of the classic theory. From now on we concentrate on the case associated with the reduced formulation. The following result is a consequence of the convergence in norm between  $\mathbf{T}$  and  $\mathbf{T}_h$ , and states that the method does not introduce spurious eigenvalues.

**Theorem 4.1.** *Let  $V \subset \mathbb{C}$  be an open set containing  $\text{sp}(\mathbf{T})$ . Then, there exists  $h_0 > 0$  such that  $\text{sp}(\mathbf{T}_h) \subset V$  for all  $h < h_0$ .*

We recall the definition of the resolvent operator of  $\mathbf{T}$  and  $\mathbf{T}_h$  respectively:

$$\begin{aligned} (z\mathbf{I} - \mathbf{T})^{-1} : \mathbf{Q}^u &\rightarrow \mathbf{Q}^u, & z \in \mathbb{C} \setminus \text{sp}(\mathbf{T}), \\ (z\mathbf{I} - \mathbf{T}_h)^{-1} : \mathbf{Q}_h^u &\rightarrow \mathbf{Q}_h^u, & z \in \mathbb{C} \setminus \text{sp}(\mathbf{T}_h). \end{aligned}$$

As a consequence of Corollary 3.1, if  $\kappa \in (0, 1)$  is an isolated eigenvalue of  $\mathbf{T}$  with multiplicity  $m$ , and  $\mathcal{E}$  its associated eigenspace, then, there exist  $m$  eigenvalues  $\kappa_h^{(1)}, \dots, \kappa_h^{(m)}$  of  $\mathbf{T}_h$ , repeated according to their respective multiplicities, which converge to  $\kappa$ . Let  $\mathcal{E}_h$  be the direct sum of their corresponding associated eigenspaces (see [16]).

We recall the definition of the *gap*  $\widehat{\delta}$  between two closed subspaces  $\mathcal{X}$  and  $\mathcal{Y}$  of  $L^2(\Omega)$ :

$$\widehat{\delta}(\mathcal{X}, \mathcal{Y}) := \max \{ \delta(\mathcal{X}, \mathcal{Y}), \delta(\mathcal{Y}, \mathcal{X}) \},$$

where

$$\delta(\mathcal{X}, \mathcal{Y}) := \sup_{x \in \mathcal{X}: \|x\|_{0,\Omega}=1} \left( \inf_{y \in \mathcal{Y}} \|x - y\|_{0,\Omega} \right).$$

**Theorem 4.2.** *There exists strictly positive constant  $C$ , such that*

$$\widehat{\delta}(\mathcal{E}, \mathcal{E}_h) \lesssim h^{\min\{s,k+1\}} \quad \text{and} \quad |\mu - \mu_h(i)| \lesssim h^{\min\{s,k+1\}}.$$

*Proof.* As consequence of Corollary 3.1,  $\mathbf{T}_h$  converges in norm to  $\mathbf{T}$  as  $h$  goes to zero. Then, the proof follows as a direct consequence of [2, Theorem 7.1 and Theorem 7.3] and using the regularity from Theorem 2.1.  $\square$

The next result provides a double order of convergence for the eigenvalues.

**Theorem 4.3.** *There exists a strictly positive constant  $h_0$  such that, for  $h < h_0$  there holds*

$$|\lambda - \lambda_h| \lesssim h^{2\min\{s,k+1\}},$$

where the hidden constant is independent of  $h$ .

*Proof.* Let  $(\lambda, \boldsymbol{\sigma}, \mathbf{u})$  solution of problem (2.11)–(2.12) and let  $(\lambda_h, \boldsymbol{\sigma}_h, \mathbf{u}_h)$  be solution of problem (3.26)–(3.27) with  $\|\mathbf{u}_h\|_{0,\Omega} = 1$ . For simplicity, we define

$$\mathbf{U} := (\boldsymbol{\sigma}, \mathbf{u}), \quad \mathbf{U}_h := (\boldsymbol{\sigma}_h, \mathbf{u}_h), \quad \mathbf{V} := (\boldsymbol{\tau}, \mathbf{v}), \quad \mathbf{V}_h := (\boldsymbol{\tau}_h, \mathbf{v}_h).$$

Then, we rewrite problems (2.11)–(2.12) and (3.26)–(3.27) as follows: Find  $(\lambda, \mathbf{U})$  and  $(\lambda_h, \mathbf{U}_h)$  solutions of the following eigenvalue problems

$$A(\mathbf{U}, \mathbf{V}) = \lambda(\mathbf{u}, \mathbf{v}), \quad A(\mathbf{U}_h, \mathbf{V}_h) = \lambda_h(\mathbf{u}_h, \mathbf{v}_h),$$

where  $A(\cdot, \cdot)$  is the symmetric and bounded bilinear forms defined by

$$A(\mathbf{U}, \mathbf{V}) = A((\boldsymbol{\sigma}, \mathbf{u}), (\boldsymbol{\tau}, \mathbf{v})) := a_0(\boldsymbol{\sigma}, \boldsymbol{\tau}) + b(\boldsymbol{\tau}, \mathbf{u}) + b(\boldsymbol{\sigma}, \mathbf{v}).$$

Moreover, we have the following classic identity

$$(\lambda - \lambda_h)(\mathbf{u}_h, \mathbf{u}_h) = A(\mathbf{U} - \mathbf{U}_h, \mathbf{U} - \mathbf{U}_h) + \lambda(\mathbf{u} - \mathbf{u}_h, \mathbf{u} - \mathbf{u}_h).$$

The proof is completed by taking absolute value on both sides of the above equation, the triangular inequality, and the approximation properties (3.21)–(3.23), together with the additional regularity provided by Theorem 2.1.  $\square$

## 5. NUMERICAL EXPERIMENTS

In this section we report some numerical tests in order to assess the performance of the proposed mixed element method, in the computation of the eigenvalues of problem (3.24)–(3.25). In all our experiments we consider the boundary condition  $\mathbf{u} = 0$  and  $\mu = 1/2$ .

We have implemented the discrete eigenvalue problem in a FEniCS code and the orders of convergence have been computed with a least-square fitting.

The schemes are performed in different domains as bidimensional convex and non convex domains and a three dimensional domain. For all the geometric configurations we compute the lowest eigenvalues and convergence orders. For the two dimensional domains we prove the schemes with polynomials degrees  $k = 0, 1, 2$  and

for the 3-D domain only for  $k = 0$  due to the machine memory. With the computed results at hand, we compare the schemes that only differ on the  $H(\text{div})$  finite element space. In particular, in the first test we show that the reduced scheme (3.26)–(3.27) gives the same numerical results as (3.24)–(3.25). This allows to perform the rest of the tests by choosing only one of them, that in our case is (3.24)–(3.25).

In each test we also report plots of the associated eigenfunctions, in particular the velocity fields and pressure fluctuations. Moreover, in several experiments we consider the relative errors  $e_{\lambda_i}$   $i = 1, 2, 3, 4$  for different choices of  $k$ , where

$$e_{\lambda_i} := \frac{|\lambda_{h_i} - \lambda_{extr_i}|}{|\lambda_{extr_i}|}.$$

Finally, we denote by  $e_{\lambda_i}(\text{RT})$  and  $e_{\lambda_i}(\text{BDM})$  the relative errors obtained using  $[\mathbb{P}_k]^n\text{-}\mathbb{P}_k\text{-RT}_k$  and  $[\mathbb{P}_k]^n\text{-}\mathbb{P}_k\text{-BDM}_{k+1}$  schemes, respectively.

**5.1. Test 1: Square.** In this test we consider as computational domain the square  $\Omega_S := (-1, 1)^2$  and the meshes for the following tests are like the presented in Figure 1.

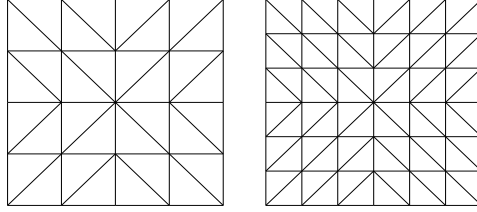


FIGURE 1. Examples of the meshes used in the unit square. The left figure represents a mesh for  $N = 4$  and the right one for  $N = 6$ .

We observe that the convexity of this domain is convex, leads to the sufficiently smooth eigenfunctions for the Stokes eigenvalue problem. This fact implies that the order of convergence will be optimal. For this test, we have considered as polynomial degrees  $k = 0, 1, 2$  together with the studied numerical schemes.



$k$	$N = 10$	$N = 20$	$N = 30$	$N = 40$	Order	$\lambda_{extr}$	[21]	[20]
0	12.61618	12.96634	13.03637	13.05313	2.00	13.08484	13.0860	13.086
	21.08840	22.63791	22.85202	22.93446	2.40	22.99702	23.0308	23.031
	21.33183	22.69036	22.88083	22.93810	2.46	22.99245	23.0308	23.031
	27.96811	31.27226	31.70100	31.81983	2.59	31.93357	32.0443	32.053
	33.42538	37.66786	38.18478	38.32443	2.69	38.44565	38.5252	38.532
1	13.08698	13.08620	13.08617	13.08617	4.56	13.08617	13.0860	13.086
	23.04310	23.03182	23.03123	23.03114	4.04	23.03109	23.0308	23.031
	23.04310	23.03182	23.03123	23.03114	4.04	23.03109	23.0308	23.031
	32.07944	32.05400	32.05270	32.05249	4.07	32.05239	32.0443	32.053
	38.60095	38.53594	38.53227	38.53165	3.92	38.53134	38.5252	38.532
2	13.08528	13.08616	13.08617	13.08617	5.84	13.08617	13.0860	13.086
	23.03116	23.03109	23.03109	23.03109	6.00	23.03109	23.0308	23.031
	23.03116	23.03109	23.03109	23.03109	6.00	23.03109	23.0308	23.031
	32.05268	32.05239	32.05239	32.05239	6.00	32.05239	32.0443	32.053
	38.53256	38.53138	38.53136	38.53136	5.97	38.53136	38.5252	38.532

TABLE 1. Lowest computed eigenvalues for polynomial degrees  $k = 0, 1, 2$  with the  $[\mathbb{P}_k]^n\text{-}\mathbb{P}_k\text{-}\mathbb{RT}_k$  scheme.

$k$	$N = 10$	$N = 20$	$N = 30$	$N = 40$	Order	$\lambda_{extr}$	[21]	[20]
0	13.18205	13.10744	13.09534	13.09127	2.21	13.08688	13.0860	13.086
	22.59086	22.92419	22.98366	23.00442	2.06	23.02944	23.0308	23.031
	22.59086	22.92419	22.98366	23.00442	2.06	23.02944	23.0308	23.031
	31.52148	31.92201	31.99384	32.01930	2.04	32.05042	32.0443	32.053
	36.97903	38.18216	38.37946	38.44657	2.19	38.51958	38.5252	38.532
1	13.08698	13.08620	13.08617	13.08617	4.56	13.08617	13.0860	13.086
	23.04310	23.03182	23.03123	23.03114	4.04	23.03122	23.0310	23.031
	23.04310	23.03182	23.03123	23.03114	4.04	23.03109	23.0308	23.031
	32.07944	32.05400	32.05270	32.05249	4.07	32.05239	32.0443	32.053
	38.60095	38.53594	38.53227	38.53165	3.92	38.53134	38.5252	38.532
2	13.08615	13.08617	13.08617	13.08617	4.75	13.08617	13.0860	13.086
	23.03116	23.03109	23.03109	23.03109	6.00	23.03109	23.0308	23.031
	23.03116	23.03109	23.03109	23.03109	6.00	23.03110	23.0308	23.031
	32.05268	32.05239	32.05239	32.05239	6.00	32.05239	32.0443	32.053
	38.53256	38.53138	38.53136	38.53136	5.92	38.53136	38.5252	38.532

TABLE 2. Lowest computed eigenvalues for polynomial degrees  $k = 0, 1, 2$  with the  $[\mathbb{P}_k]^n\text{-}\mathbb{RT}_k$  scheme.

$k$	$N = 10$	$N = 20$	$N = 30$	$N = 40$	Order	$\lambda_{extr}$	[21]	[20]
0	13.39520	13.16477	13.12123	13.10591	1.97	13.08574	13.0860	13.086
	23.74378	23.22000	23.11593	23.07899	1.89	23.02641	23.0308	23.031
	24.19514	23.32856	23.16384	23.10587	1.96	23.02865	23.0308	23.031
	33.73344	32.50272	32.25523	32.16703	1.87	32.03920	32.0443	32.053
	41.15209	39.23059	38.84532	38.70858	1.88	38.51262	38.5252	38.532
1	13.08919	13.08636	13.08621	13.08618	3.99	13.08617	13.0860	13.086
	23.04441	23.03195	23.03126	23.03115	3.96	23.03109	23.0308	23.031
	23.05331	23.03253	23.03138	23.03118	3.95	23.03109	23.0308	23.031
	32.10055	32.0555	32.05302	32.05259	3.92	32.05238	32.0443	32.053
	38.61259	38.53671	38.53243	38.53170	3.92	38.53134	38.5252	38.532
2	13.08618	13.08617	13.08617	13.08617	6.16	13.08617	13.0860	13.086
	23.03117	23.03109	23.03109	23.03109	6.04	23.03109	23.0308	23.031
	23.03128	23.03110	23.03109	23.03109	6.01	23.03109	23.0308	23.031
	32.05303	32.05240	32.05239	32.05239	6.02	32.05239	32.0443	32.053
	38.53239	38.53138	38.53136	38.53136	5.92	38.53136	38.5252	38.532

TABLE 3. Lowest computed eigenvalues for polynomial degrees  $k = 1, 2, 3$ . with the  $[\mathbb{P}_k]^n\text{-}\mathbb{P}_k\text{-BDM}_{k+1}$  scheme.

$k$	$N = 10$	$N = 20$	$N = 30$	$N = 40$	Order	$\lambda_{extr}$	[21]	[20]
0	13.46029	13.18088	13.12837	13.10993	1.98	13.08589	13.0860	13.086
	24.18596	23.32433	23.16178	23.10467	1.97	23.02910	23.0308	23.031
	24.18596	23.32433	23.16178	23.10467	1.97	23.02910	23.0308	23.031
	34.23489	32.61702	32.30485	32.19470	1.94	32.04581	32.0443	32.053
	41.75299	39.35261	38.89728	38.73736	1.96	38.52295	38.5252	38.532
1	13.08997	13.08642	13.08622	13.08618	3.93	13.08617	13.0860	13.086
	23.05092	23.03240	23.03135	23.03118	3.92	23.03109	23.0308	23.031
	23.05092	23.03240	23.03135	23.03118	3.92	23.03109	23.0308	23.031
	32.10848	32.05619	32.05315	32.05263	3.88	32.05237	32.0443	32.053
	38.61788	38.53707	38.53250	38.53172	3.92	38.53134	38.5252	38.532
2	13.08619	13.08617	13.08617	13.08617	6.09	13.08617	13.0860	13.086
	23.03128	23.03110	23.03109	23.03109	5.97	23.03109	23.0308	23.031
	23.03128	23.03110	23.03109	23.03109	5.97	23.03109	23.0308	23.031
	32.05323	32.05240	32.05239	32.05239	5.91	32.05239	32.0443	32.053
	38.53245	38.53138	38.53136	38.53136	5.92	38.53136	38.5252	38.532

TABLE 4. Lowest computed eigenvalues for polynomial degrees  $k = 1, 2, 3$ . with the  $[\mathbb{P}_k]^n\text{-BDM}_{k+1}$  scheme.

In Table 1 we report the first five eigenvalues computed with the  $[\mathbb{P}_k]^n\text{-}\mathbb{P}_k\text{-RT}_k$  scheme, considering different meshes and polynomial degrees. In the column  $\lambda_{extr}$  we report extrapolated values, obtained with a least square fitting, which we compare with two very well known references that have deal with the same domain. We observe that our extrapolated values are close to those in [21, 20] and that the rates of convergence are as we expect. In fact, we notice that for  $k = 0$ , the order of approximation is clearly  $h^2$ , meanwhile for  $k > 0$  the observed order is close to  $h^{2(k+1)}$ . This increased order is expectable for high order methods, as it happen, for example, in DG methods (see for instance [8, 18]). In Table 2, the results from using the  $[\mathbb{P}_k]^n\text{-RT}_k$  scheme are provided. We observe that similar results are obtained when compared with the results from Table 1.

On the other hand, Table 3 shows the computed eigenvalues when using the  $[\mathbb{P}_k]^n\text{-}\mathbb{P}_k\text{-BDM}_{k+1}$  scheme, where we observe that an optimal rate of convergence  $O(h^{2(k+1)})$  is reached for high order elements. For instance, in Figure 3 we observe that, except for the noise present in the error slopes, the scheme allows to stay on the optimal rate of convergence. This is compared with Table 4, where we have the computed eigenvalues from the  $[\mathbb{P}_k]^n\text{-BDM}_{k+1}$  scheme. As before, the results are considerably similar with those from Table 3. Hence, we conclude that, although the full and reduced numerical schemes studied are not equivalent, they yield to the same numerical results. To complete the experiment, we present in Figure 2 the first, third and fourth lowest computed eigenfunctions on the square domain, and in Figure 3 we present the error behavior on the chosen numerical schemes.

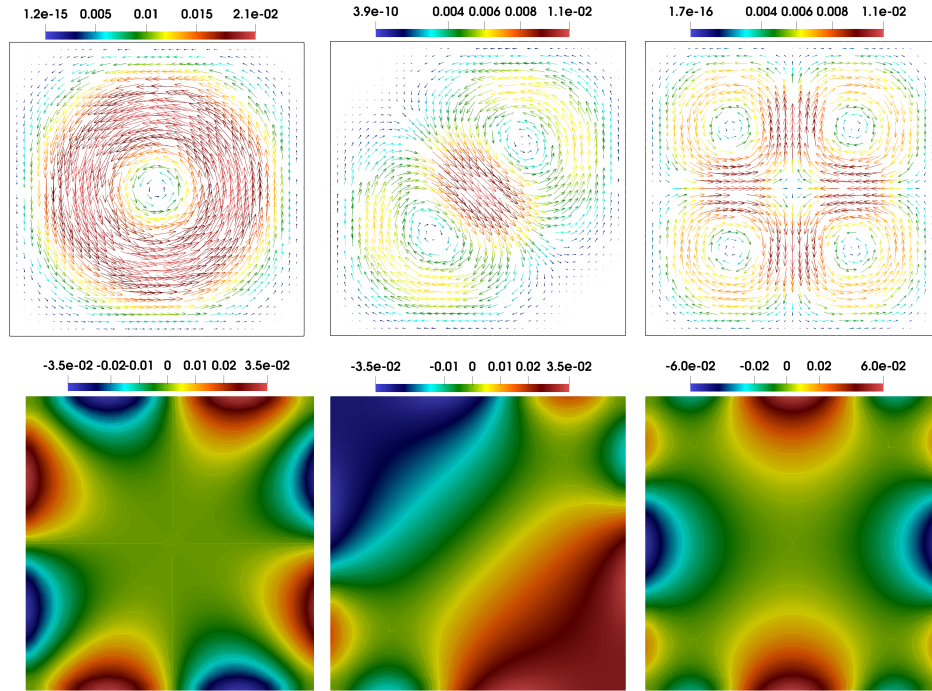


FIGURE 2. Approximate velocity field  $u_h$  (top row) and pressure  $p_h$  (bottom row), corresponding to the first, third and fourth lowest eigenvalues in the square domain.

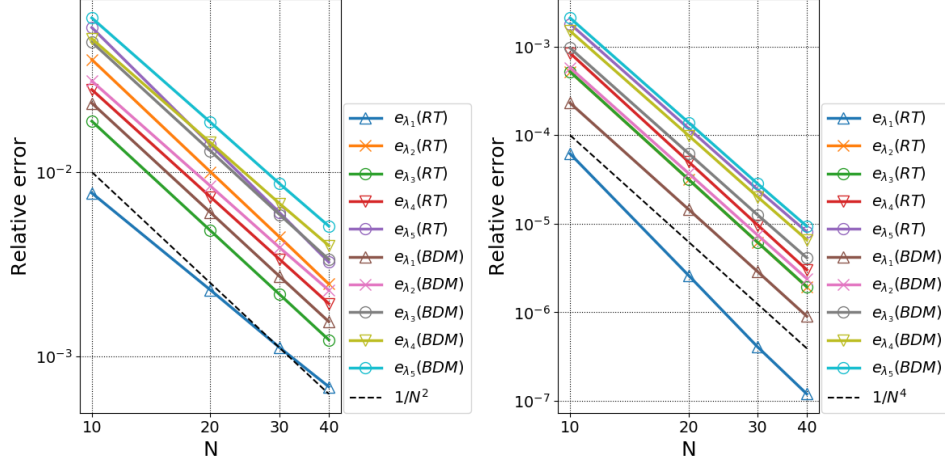


FIGURE 3. Comparison of the eigenvalues error behavior in the square domain when using  $[\mathbb{P}_k]^n\text{-}\mathbb{P}_k\text{-RT}_k$  and  $[\mathbb{P}_k]^n\text{-}\mathbb{P}_k\text{-BDM}_{k+1}$  schemes. The experiment considers polynomials of degree  $k = 0$  (left) and  $k = 1$  (right).

**5.2. Test 2: Circular domain.** In this test we consider the unitary circle as computational domain, which we define by  $\Omega_C := \{(x, y) \in \mathbb{R}^2 : x^2 + y^2 \leq 1\}$ . The relevance of this experiment is that we are approximating a curved domain with triangular meshes, which lead to a variational crime. In Figure 4 we present examples of the quasi-uniform triangular meshes considered to approximate the circular domain.

The fact that we are approximating a curved domain by means of a polygonal one is reflected in the numerical experiments presented below in Table 5 where, independent of the polynomial degree, the order of convergence is  $\mathcal{O}(h^2)$  for all  $k \geq 0$ .

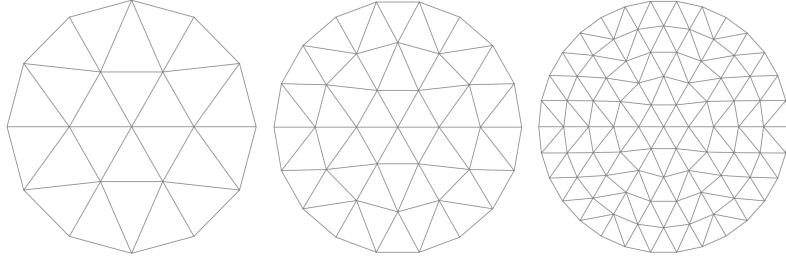


FIGURE 4. Meshes used in the circular domain.

The results from using the  $[\mathbb{P}_k]^n\text{-}\mathbb{P}_k\text{-BDM}_{k+1}$  scheme are described in Table 6, where similar rates of convergence are observed. We recall that, in both cases,  $N$  represents the mesh resolution such that the number of elements is  $6N^2$ . In Figure 5 we present the approximated eigenfunctions for the lowest frequencies. We further

describe the results obtained in Figure 6, where we observe the experimental rates obtained, which are in good agreement with those predicted by theory.

$k$	$N = 20$	$N = 30$	$N = 40$	$N = 50$	Order	$\lambda_{extr}$	[18]
0	14.94827	14.79867	14.74712	14.72354	2.04	14.68251	14.68345
	26.81747	26.56803	26.48211	26.44329	2.05	26.37559	26.37840
	26.81821	26.56845	26.48262	26.44365	2.06	26.37683	26.37862
	41.32838	40.98177	40.85915	40.80453	2.01	40.70533	40.71434
	41.34096	40.98359	40.86093	40.80487	2.05	40.70809	40.71606
1	14.94196	14.79448	14.74448	14.72169	2.08	14.68323	14.68345
	26.84091	26.57657	26.48686	26.44594	2.08	26.37704	26.37840
	26.84099	26.57662	26.48687	26.44595	2.08	26.37703	26.37862
	41.42501	41.01797	40.87964	40.81652	2.08	40.71046	40.71434
	41.42543	41.01805	40.87966	40.81654	2.08	40.71037	40.71606
2	14.94315	14.79487	14.74464	14.72177	2.09	14.68361	14.68345
	26.84301	26.57727	26.48715	26.44610	2.08	26.37680	26.37840
	26.84303	26.57728	26.48716	26.44610	2.08	26.37680	26.37862
	41.42807	41.01900	40.88008	40.81675	2.08	40.71012	40.71434
	41.42814	41.01902	40.88008	40.81676	2.08	40.71010	40.71606

TABLE 5. Lowest computed eigenvalues for polynomial degrees  $k = 0, 1, 2$ , using the  $[\mathbb{P}_k]^n$ - $\mathbb{P}_k$ - $\mathbb{RT}_k$  scheme.

$k$	$N = 20$	$N = 30$	$N = 40$	$N = 50$	Order	$\lambda_{extr}$	[18]
0	14.82469	14.71768	14.69784	14.69090	2.00	14.68199	14.68345
	26.77392	26.47427	26.41889	26.39951	2.00	26.37450	26.37840
	26.77392	26.47427	26.41889	26.39951	2.00	26.37450	26.37862
	41.56881	40.92423	40.80343	40.76105	1.98	40.70545	40.71434
	41.56881	40.92423	40.80343	40.76105	1.98	40.70545	40.71606
1	14.70933	14.68872	14.68496	14.68365	2.02	14.68199	14.68345
	26.42481	26.38682	26.38000	26.37764	2.05	26.37473	26.37840
	26.42481	26.38682	26.38000	26.37764	2.05	26.37703	26.37862
	40.78741	40.72552	40.71483	40.71115	2.11	40.70686	40.71434
	40.78741	40.72552	40.71483	40.71115	2.11	40.70686	40.71606
2	14.70930	14.68873	14.68496	14.68365	2.02	14.68200	14.68345
	26.42370	26.38677	26.38000	26.37764	2.02	26.37467	26.37840
	26.42370	26.38677	26.38000	26.37764	2.02	26.37467	26.37862
	40.78222	40.72523	40.71478	40.71113	2.02	40.70655	40.71434
	40.78222	40.72523	40.71478	40.71113	2.02	40.70655	40.71606

TABLE 6. Lowest computed eigenvalues for polynomial degrees  $k = 0, 1, 2$ , when using the  $[\mathbb{P}_k]^n$ - $\mathbb{P}_k$ - $\mathbb{BDM}_{k+1}$  scheme.

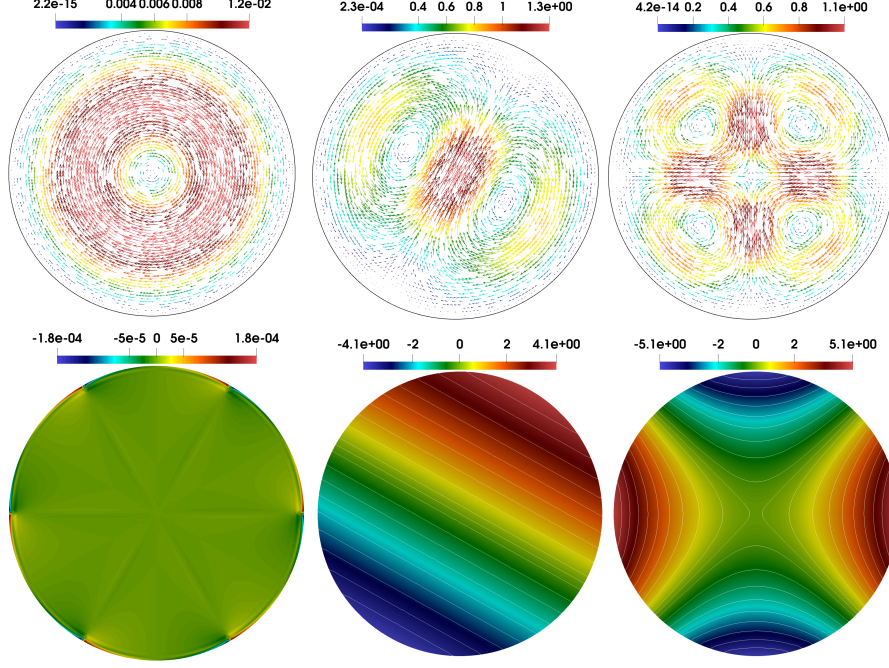


FIGURE 5. Approximate velocity field  $\mathbf{u}_h$  (top row) and pressure  $p_h$  (bottom row), corresponding to the first, third and fourth lowest eigenvalues in the unit circular domain.

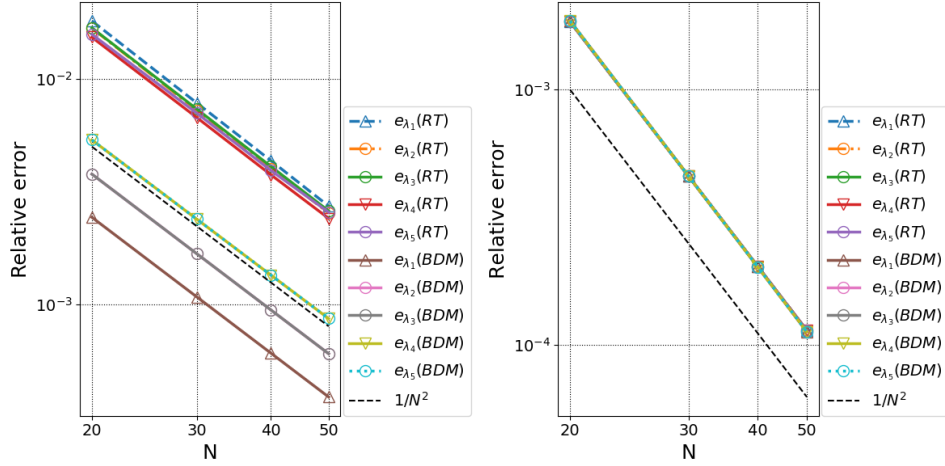


FIGURE 6. Comparison of the eigenvalues error behavior in the circle when using  $[\mathbb{P}_k]^n\text{-}\mathbb{P}_k\text{-RT}_k$  and  $[\mathbb{P}_k]^n\text{-}\mathbb{P}_k\text{-BDM}_{k+1}$  schemes. The experiment considers polynomials of degree  $k = 0$  (left) and  $k = 2$  (right).

**5.3. Test 3. The L-Shape domain.** In this numerical test we consider an L-shape domain given by  $\Omega_L := (-1, 1) \times (-1, 1) \setminus [-1, 0] \times [-1, 0]$ . In Table 7 we report the results when using  $[\mathbb{P}_k]^n\text{-}\mathbb{P}_k\text{-RT}_k$  and  $[\mathbb{P}_k]^n\text{-}\mathbb{P}_k\text{-BDM}_{k+1}$  schemes to solve the discrete eigenvalue problem. The table shows the corresponding order of convergence together with the extrapolated values of the five lowest computed eigenvalues. Note that the singularity produced by the reentrant corner yields to a rate of convergence around 1.7 (see [20] for instance), as can be seen in the lowest computed eigenvalue. In fact, we observe that the order of convergence is  $s \approx 2 \min\{r, k+1\}$ , with  $1.7 \leq r \leq 2$ , as is predictable in this geometry. For better visualization, we explore this result in the relative error plots in Figure 7, where the slopes are compared with the  $1/N^{\sqrt{3}}$ , which is the best order possible with uniform refinement.

We end this test reporting plots of the velocity fields and pressure fluctuations in Figure 8, where, as is expectable, high gradients around the singularity are observed.

Scheme	$N = 9$	$N = 15$	$N = 20$	$N = 35$	Order	$\lambda_{extr}$
$[\mathbb{P}_k]^n\text{-}\mathbb{P}_k\text{-RT}_k$	29.43565	30.83700	31.16193	31.62598	1.59	31.89457
	34.98077	36.28132	36.50660	36.83669	2.03	36.94231
	40.70064	41.43833	41.62290	41.83014	1.73	41.94524
	46.83830	48.22776	48.47328	48.80875	2.07	48.91635
	52.08483	53.96541	54.48404	55.02474	1.65	55.37238
$[\mathbb{P}_k]^n\text{-}\mathbb{P}_k\text{-BDM}_{k+1}$	32.59542	32.24970	32.14635	32.06144	1.75	32.00483
	38.76953	37.57884	37.32081	37.11240	2.26	37.03276
	44.76985	42.88018	42.46067	42.10765	2.19	41.96744
	52.09587	50.19205	49.67367	49.20827	1.81	48.93475
	58.84979	56.72442	56.20364	55.63553	1.79	55.33628

TABLE 7. Lowest computed eigenvalues for polynomial degrees  $k = 0$  in the L-shape domain.

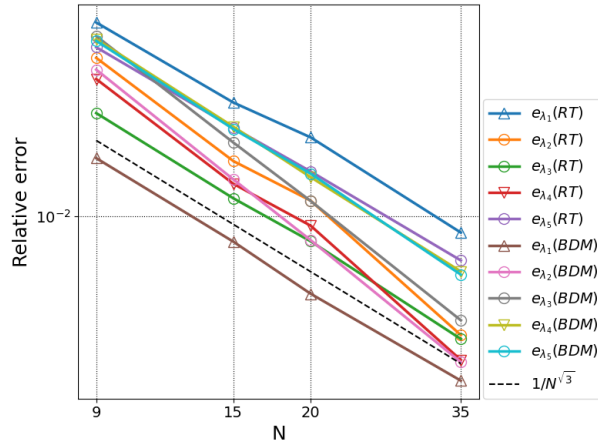


FIGURE 7. Comparison of the eigenvalues error behavior in the L-shape domain when using  $[\mathbb{P}_k]^n\text{-}\mathbb{P}_k\text{-RT}_k$  and  $[\mathbb{P}_k]^n\text{-}\mathbb{P}_k\text{-BDM}_{k+1}$  schemes. The experiment considers polynomials of degree  $k = 0$ .

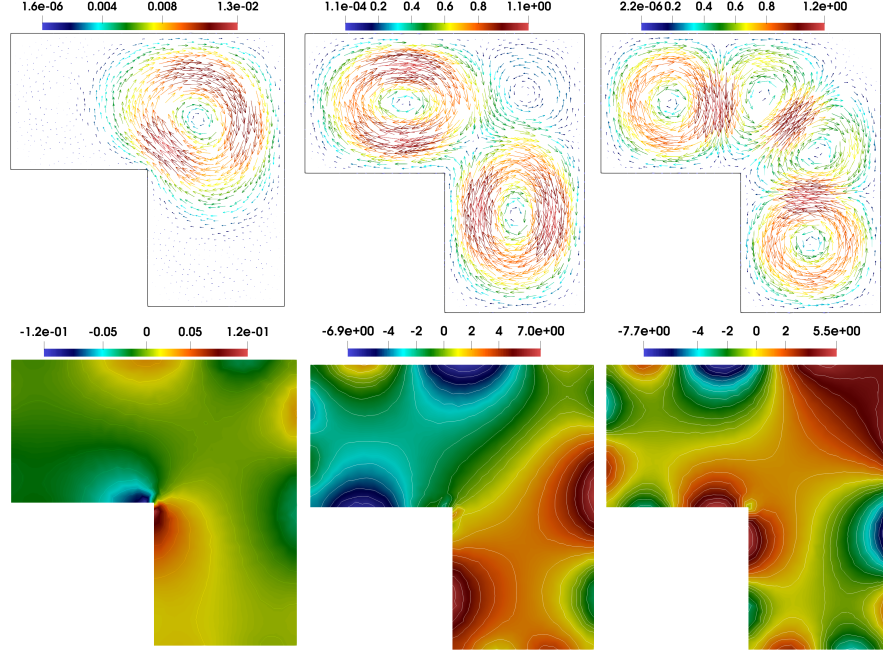


FIGURE 8. Approximate velocity field  $u_h$  (top row) and pressure  $p_h$  (bottom row), corresponding to the first, third and fourth lowest eigenvalues in the L-shape domain.

**5.4. 3-D test: Cubic and spherical domain.** In this test we further assess the proposed schemes by consider two different three dimensional scenarios. The first case considers cube in the region  $\Omega = (0, 1)^3$ . Here,  $N$  represents the number of cell per side such that the number of tetrahedron is  $6(N + 1)^3$ . In Figure 9 we present examples of the meshes used in the cube domain.

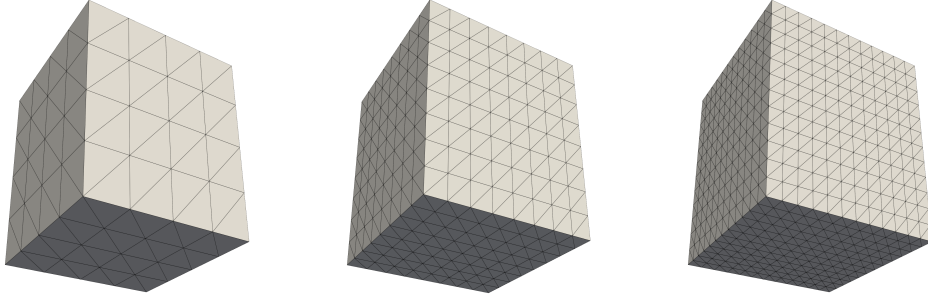


FIGURE 9. Examples of the meshes used in the unit cube. The left figure represents a mesh for  $N = 4$ , the figure in for  $N = 8$  and the right figure for  $N = 12$ .



In the second scenario we consider the unitary sphere

$$\Omega_S := \{(x, y, z) \in \mathbb{R}^3 : x^2 + y^2 + z^2 \leq 1\}.$$

For this case,  $N$  represents the mesh resolution such that  $N \sim 1/h$ . We remark that this test consists into approximate a curved domain by means of tetrahedral meshes. In Figure 10 we present several meshes used in the experiment.

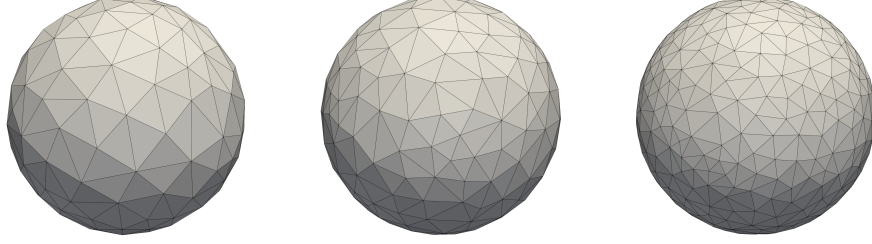


FIGURE 10. Examples of the meshes used in the unitary sphere. The left figure represents a mesh for  $N = 8$ , the middle figure for  $N = 10$  and the right figure for  $N = 14$ .

For simplicity, both scenarios only consider the lowest order of approximation ( $k = 0$ ).

For the unit cube, the results from using the  $[\mathbb{P}_k]^n\text{-}\mathbb{P}_k\text{-RT}_k$  and  $[\mathbb{P}_k]^n\text{-}\mathbb{P}_k\text{-BDM}_{k+1}$  numerical schemes are reported in Table 8. In figure 11 we present the relative error plot for the approximated eigenvalues compared with the extrapolated ones on each table. It notes that the expected rate of convergence is observed. Together with this, the second and fourth lowest eigenfunctions corresponding to  $\mathbf{u}_h$  and  $p_h$  are depicted in Figure 12.

On the other hand, the unit sphere case is described in Table 9. Here, we show that the proposed methods work perfectly and deliver the expected double order of convergence for both schemes, which is observed in Figure 13. For completeness, in Figure 14 we present plots of the approximated velocity fields and pressure fluctuations associated with the second and fourth lowest eigenvalues. As in the circular domain, we observe an equally pressure distribution on the boundary for the second eigenvalue.

Scheme	$N = 6$	$N = 8$	$N = 10$	$N = 12$	Order	$\lambda_{extr}$
$[\mathbb{P}_k]^n\text{-}\mathbb{P}_k\text{-RT}_k$	62.35998	62.23777	62.19632	62.18064	3.29	62.15973
	62.69715	62.42145	62.31185	62.25999	2.60	62.17340
	62.69715	62.42145	62.31185	62.25999	2.60	62.17340
	84.69821	89.79683	91.41328	91.49049	4.33	91.99133
	89.14796	91.13378	92.15949	91.49049	5.43	91.86755
$[\mathbb{P}_k]^n\text{-}\mathbb{P}_k\text{-BDM}_{k+1}$	65.90006	64.32034	63.56386	63.14558	1.88	62.11709
	66.63208	64.74326	63.83797	63.33726	1.88	62.10739
	66.63208	64.74326	63.83797	63.33726	1.88	62.10739
	100.1074	96.65063	94.93243	93.96083	1.75	91.35751
	100.1074	96.65063	94.93243	93.96083	1.75	91.35751

TABLE 8. Lowest computed eigenvalues for polynomial degrees  $k = 0$  in the unit cube domain.

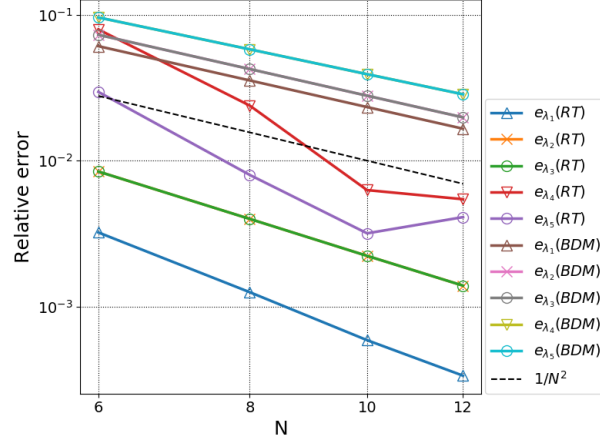


FIGURE 11. Comparison of the relative error behavior in the unit cube when using  $[\mathbb{P}_k]^n\text{-}\mathbb{P}_k\text{-RT}_k$  and  $[\mathbb{P}_k]^n\text{-}\mathbb{P}_k\text{-BDM}_{k+1}$  schemes. The experiment considers polynomials of degree  $k = 0$ .

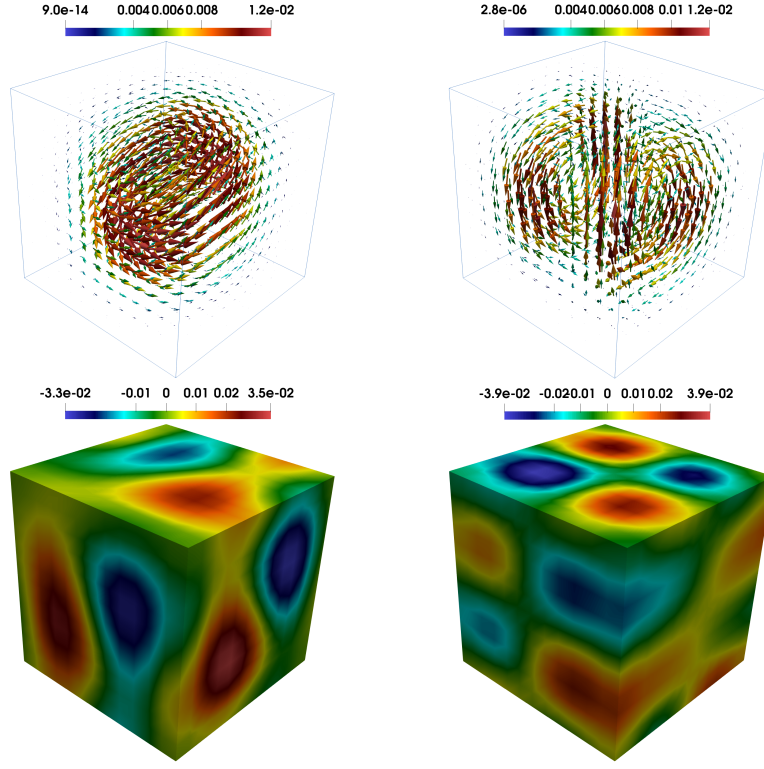


FIGURE 12. Approximated velocity field  $\mathbf{u}_h$  (top) and pressure  $p$  (bottom), corresponding to the second and fourth lowest eigenvalues in the unit cube domain.

Scheme	$N = 8$	$N = 10$	$N = 12$	$N = 14$	Order	$\lambda_{extr}$
$[\mathbb{P}_k]^n\text{-}\mathbb{P}_k\text{-RT}_k$	21.20335	20.92074	20.75254	20.65936	1.83	20.35082
	21.21249	20.93014	20.75649	20.66213	1.76	20.32925
	21.26202	20.93587	20.76475	20.66667	2.21	20.42274
	32.88974	33.16111	33.37782	33.40790	2.30	33.63347
	32.92827	33.19610	33.38327	33.42272	2.43	33.61269
$[\mathbb{P}_k]^n\text{-}\mathbb{P}_k\text{-BDM}_{k+1}$	22.25623	21.60098	21.21005	20.99626	1.85	20.29349
	22.26758	21.61050	21.21633	21.00327	1.85	20.29719
	22.31279	21.64527	21.24160	21.00398	1.68	20.42274
	37.33594	35.95812	35.22679	34.82632	2.24	33.81667
	37.35343	36.01392	35.23896	34.83680	2.03	33.62683

TABLE 9. Lowest computed eigenvalues for polynomial degrees  $k = 0$  in the unit sphere domain.

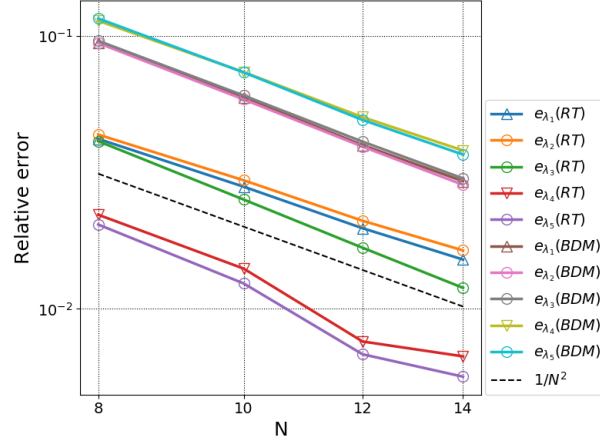


FIGURE 13. Comparison of the relative error behavior in the unit sphere when using  $[\mathbb{P}_k]^n\text{-}\mathbb{P}_k\text{-RT}_k$  and  $[\mathbb{P}_k]^n\text{-}\mathbb{P}_k\text{-BDM}_{k+1}$  schemes. The experiment considers polynomials of degree  $k = 0$ .

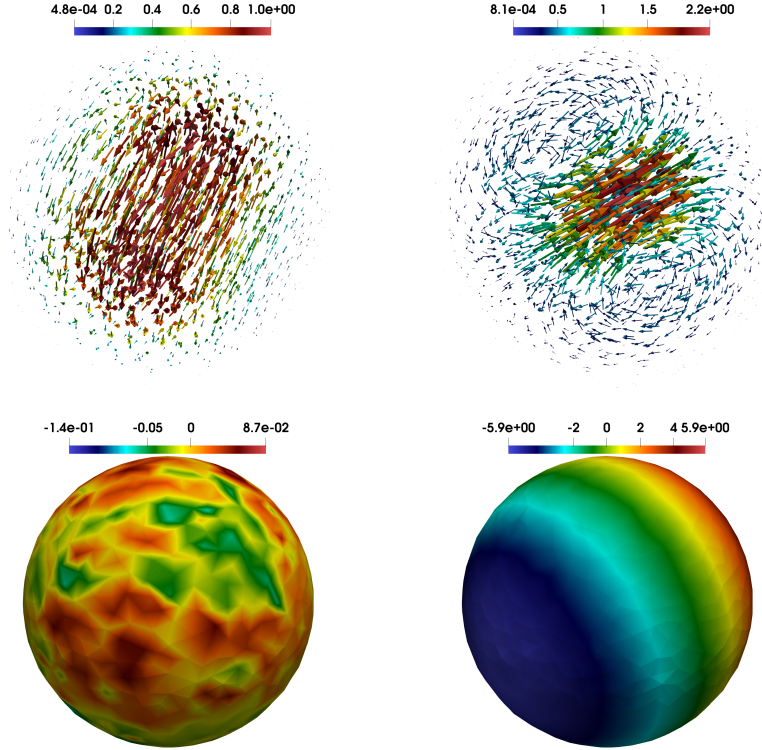


FIGURE 14. Approximated velocity field  $\mathbf{u}_h$  (top) and pressure  $p_h$  (bottom), corresponding to the second and fourth lowest eigenvalues in the unit sphere domain.

## 6. CONCLUSIONS

From our analysis and numerical tests, we derive the following conclusions:

- The introduction of the pseudo-stress tensor allowed to propose a mixed finite element formulation for a Stokes eigenvalue problem that do not introduce spurious modes, and the analysis was possible thanks to definition of appropriate solution operators. This allowed to obtain the respective approximation results along with theoretical convergence rates based on well-known finite element spaces.
- The numerical schemes employed in our study perform an accurate approximation of the eigenvalues and the associated eigenfunctions in two and three dimensions.
- For curved domains both methods works perfectly, even from the fact that we are considering polygonal/polyhedral meshes, depending in the dimension fo the domain.
- For the lowest order in both numerical schemes ( $k = 0$ ) the double order of convergence is clearly quadratic and, for  $k \geq 1$ , the  $[\mathbb{P}_k]^n\text{-}\mathbb{P}_k\text{-BDM}_{k+1}$  scheme seems to be more stable than the  $[\mathbb{P}_k]^n\text{-}\mathbb{P}_k\text{-RT}_k$  when the order fo convergence are computed. This is due the fact that, when  $[\mathbb{P}_k]^n\text{-}\mathbb{P}_k\text{-RT}_k$  is considered, the computed eigenvalues are more close between them than the scheme with BDM elements. This phenomenon is observable in the relative error plots.
- In non convex domains, the results are the expectable due the singularity of the geometry. This is an interesting fact that motivates the analysis of adaptive schemes.

## REFERENCES

- [1] P. F. ANTONIETTI, A. BUFFA, AND I. PERUGIA, *Discontinuous Galerkin approximation of the Laplace eigenproblem*, Comput. Methods Appl. Mech. Engrg., 195 (2006), pp. 3483–3503.
- [2] I. BABUŠKA AND J. OSBORN, *Handbook of numerical analysis. Vol. II*, (1991), pp. x+928. Finite element methods. Part 1.
- [3] L. BEIRÃO DA VEIGA, F. BREZZI, L. D. MARINI, AND A. RUSSO, *Mixed virtual element methods for general second order elliptic problems on polygonal meshes*, ESAIM Math. Model. Numer. Anal., 50 (2016), pp. 727–747.
- [4] D. BOFFI, *Finite element approximation of eigenvalue problems*, Acta Numer., 19 (2010), pp. 1–120.
- [5] D. BOFFI, F. BREZZI, AND M. FORTIN, *Mixed finite element methods and applications*, vol. 44 of Springer Series in Computational Mathematics, Springer, Heidelberg, 2013.
- [6] F. BREZZI, J. DOUGLAS, JR., AND L. D. MARINI, *Two families of mixed finite elements for second order elliptic problems*, Numer. Math., 47 (1985), pp. 217–235.
- [7] F. BREZZI AND M. FORTIN, *Mixed and hybrid finite element methods*, vol. 15 of Springer Series in Computational Mathematics, Springer-Verlag, New York, 1991.
- [8] A. BUFFA, P. HOUSTON, AND I. PERUGIA, *Discontinuous Galerkin computation of the Maxwell eigenvalues on simplicial meshes*, J. Comput. Appl. Math., 204 (2007), pp. 317–333.
- [9] Z. CAI, C. TONG, P. S. VASSILEVSKI, AND C. WANG, *Mixed finite element methods for incompressible flow: stationary Stokes equations*, Numer. Methods Partial Differential Equations, 26 (2010), pp. 957–978.
- [10] F. GARDINI, *Mixed approximation of eigenvalue problems: a superconvergence result*, M2AN Math. Model. Numer. Anal., 43 (2009), pp. 853–865.
- [11] G. N. GATICA, A. MÁRQUEZ, AND M. A. SÁNCHEZ, *Analysis of a velocity-pressure-pseudostress formulation for the stationary Stokes equations*, Comput. Methods Appl. Mech. Engrg., 199 (2010), pp. 1064–1079.

- [12] J. GEDICKE AND A. KHAN, *Arnold-Winther mixed finite elements for Stokes eigenvalue problems*, SIAM J. Sci. Comput., 40 (2018), pp. A3449–A3469.
- [13] ———, *Divergence-conforming discontinuous Galerkin finite elements for Stokes eigenvalue problems*, Numer. Math., 144 (2020), pp. 585–614.
- [14] V. GIRAUT AND P.-A. RAVIART, *Finite element methods for Navier-Stokes equations*, vol. 5 of Springer Series in Computational Mathematics, Springer-Verlag, Berlin, 1986. Theory and algorithms.
- [15] R. HIPTMAIR, *Finite elements in computational electromagnetism*, Acta Numer., 11 (2002), pp. 237–339.
- [16] T. KATO, *Perturbation theory for linear operators*, Die Grundlehren der mathematischen Wissenschaften, Band 132, Springer-Verlag New York, Inc., New York, 1966.
- [17] F. LEPE, S. MEDDAHI, D. MORA, AND R. RODRÍGUEZ, *Mixed discontinuous Galerkin approximation of the elasticity eigenproblem*, Numer. Math., 142 (2019), pp. 749–786.
- [18] F. LEPE AND D. MORA, *Symmetric and nonsymmetric discontinuous Galerkin methods for a pseudostress formulation of the Stokes spectral problem*, SIAM J. Sci. Comput., 42 (2020), pp. A698–A722.
- [19] F. LEPE, D. MORA, AND R. RODRÍGUEZ, *Finite element analysis of a bending moment formulation for the vibration problem of a non-homogeneous Timoshenko beam*, J. Sci. Comput., 66 (2016), pp. 825–848.
- [20] C. LOVADINA, M. LYL, AND R. STENBERG, *A posteriori estimates for the Stokes eigenvalue problem*, Numer. Methods Partial Differential Equations, 25 (2009), pp. 244–257.
- [21] S. MEDDAHI, D. MORA, AND R. RODRÍGUEZ, *A finite element analysis of a pseudostress formulation for the Stokes eigenvalue problem*, IMA J. Numer. Anal., 35 (2015), pp. 749–766.
- [22] B. MERCIER, J. OSBORN, J. RAPPAP, AND P.-A. RAVIART, *Eigenvalue approximation by mixed and hybrid methods*, Math. Comp., 36 (1981), pp. 427–453.
- [23] P.-A. RAVIART AND J. M. THOMAS, *A mixed finite element method for 2nd order elliptic problems*, in Mathematical aspects of finite element methods (Proc. Conf., Consiglio Naz. delle Ricerche (C.N.R.), Rome, 1975), 1977, pp. 292–315. Lecture Notes in Math., Vol. 606.
- [24] J. E. ROBERTS AND J.-M. THOMAS, *Mixed and hybrid methods*, in Handbook of numerical analysis, Vol. II, Handb. Numer. Anal., II, North-Holland, Amsterdam, 1991, pp. 523–639.

GIMNAP-DEPARTAMENTO DE MATEMÁTICA, UNIVERSIDAD DEL BÍO - BÍO, CASILLA 5-C, CONCEPCIÓN, CHILE.

*Email address:* `flepe@ubiobio.cl`

DEPARTAMENTO DE CIENCIAS EXACTAS, UNIVERSIDAD DE LOS LAGOS, CASILLA 933, OSORNO, CHILE.

*Email address:* `gonzalo.rivera@ulagos.cl`

DEPARTAMENTO DE MATEMÁTICA, UNIVERSIDAD TÉCNICA FEDERICO SANTA MARÍA, VALPARAÍSO, CHILE.

*Email address:* `jesus.vellojinm@usm.cl`